

CERN-PH-EP-2015-330
22 December 2015

Multipion Bose-Einstein correlations in pp, p–Pb, and Pb–Pb collisions at the LHC

ALICE Collaboration*

Abstract

Three- and four-pion Bose-Einstein correlations are presented in pp, p–Pb, and Pb–Pb collisions at the LHC. We compare our measured four-pion correlations to the expectation derived from two- and three-pion measurements. Such a comparison provides a method to search for coherent pion emission. We also present mixed-charge correlations in order to demonstrate the effectiveness of several analysis procedures such as Coulomb corrections. Same-charge four-pion correlations in pp and p–Pb appear consistent with the expectations from three-pion measurements. However, the presence of non-negligible background correlations in both systems prevent a conclusive statement. In Pb–Pb collisions, we observe a significant suppression of three- and four-pion Bose-Einstein correlations compared to expectations from two-pion measurements. There appears to be no centrality dependence of the suppression within the 0–50% centrality interval. The origin of the suppression is not clear. However, by postulating either coherent pion emission or large multibody Coulomb effects, the suppression may be explained.

arXiv:1512.08902v2 [nucl-ex] 26 May 2016

1 Introduction

The last stage of particle interactions in high-energy collisions (kinetic freeze-out) occurs on the femtoscopic length scale (10^{-15} m) where quantum statistical (QS) correlations are expected. QS correlations at low relative momentum are known to be sensitive to the space-time extent (e.g. radius) and dynamics of the particle emitting source [1–3]. Another interesting, although less studied, aspect of QS correlations is the possible suppression due to coherent pion emission [4–7]. Coherent emission may arise for several reasons such as from the formation of a disoriented chiral condensate (DCC) [8–11], gluonic or pionic Bose-Einstein Condensates (BEC) [12–15], or multiple coherent sources from pulsed radiation [16].

Coherent emission is known to suppress Bose-Einstein correlations below the expectation from a fully chaotic particle emitting source. Some of the earliest attempts to search for coherence relied solely on fits to two-pion correlation functions [17]. The intercepts of the fits at zero relative momentum were found to be highly suppressed. However, it was quickly realized that Coulomb repulsion and long-lived emitters (e.g. long-lived resonance decays) also suppress the correlation function significantly. Furthermore, the precise shape of the freeze-out space-time distribution is unknown. As a consequence, the corresponding functional form of the correlation function in momentum space is also unknown. Being such, there is no reliable way to extrapolate the measured correlation function to the unmeasured intercept.

Multipion Bose-Einstein correlations could provide an increased sensitivity to coherence as the expected suppression increases with the order of the correlation function [5, 18, 19]. However, the analysis of multipion Bose-Einstein correlations comes at the expense of increased complexity. Some of the earliest attempts to measure three-pion Bose-Einstein correlations relied on a different methodology and gave rather ambiguous results [20–23]. Recently the methodology of isolating three- and four-pion Bose-Einstein correlations has been considerably improved [19]—particularly in regards to the treatment of long-lived pion emitters. Our previous measurements of three-pion correlations revealed a suppression which may arise from a coherent fraction (G) of $23\% \pm 8\%$ at low p_T at kinetic freeze-out [24].

We present three- and four-pion QS correlations in pp, p–Pb, and Pb–Pb collisions at the LHC measured with ALICE using the methodology presented in Ref. [19]. The QS correlations are extracted from the measured multipion distributions. The extraction of QS correlations relies on the treatment of long-lived pion emitters and final-state interactions (FSI), e.g. Coulomb correlations. QS correlations between pions separated by large distances ($> \sim 100$ fm) are only observable at very low relative momentum, where track merging effects and finite momentum resolution prevent reliable measurements. The effect of long-lived emitters at measurable relative momentum is to simply dilute the correlation functions. The presented correlation functions are corrected for this dilution as well as FSI and therefore should represent the pure QS correlations from short-lived pion emitters, i.e. the core of particle production. We also present the mixed-charge four-pion correlations, which are used to demonstrate the effectiveness of all corrections in the analysis procedure.

The measured multipion QS correlations require a reference in order to quantify a possible suppression. Lower order QS correlation functions form the reference in this analysis. Two-pion QS correlations, in particular, provide a direct measurement of the pair-exchange magnitudes, which may be used as a building block to form an expectation for higher order correlation functions. These “expected” multibody correlations were termed “built” in Ref. [19].

This article is organized into 7 sections. We explain the detector setup and data selection in Sec. 2. In Sec. 3, we describe the analysis methodology. The results are presented in Sec. 4. In Sec. 5, we discuss all of the systematic uncertainties investigated. We discuss several possible origins of the suppression in Sec. 6. Finally, in Sec. 7 we summarize our findings.

2 Experimental setup and data selection

Data from pp, p–Pb and Pb–Pb collisions at the LHC recorded with ALICE [25] are analyzed. The data for pp collisions at $\sqrt{s} = 7$ TeV were taken during 2010, during 2013 for p–Pb collisions at $\sqrt{s_{NN}} = 5.02$ TeV, and during 2011 for Pb–Pb at $\sqrt{s_{NN}} = 2.76$ TeV.

The trigger conditions are slightly different for each of the three collision systems. For pp collisions, at least one hit in the Silicon Pixel Detector (SPD), at central rapidity, or either of the V0 detectors [26], at forward rapidity, is required. For Pb–Pb and p–Pb collisions, the trigger is formed by requiring hits simultaneously in each V0.

The Inner Tracking System (ITS) and Time Projection Chamber (TPC) located at mid-rapidity are used for particle tracking [27]. There are 6 layers of silicon detectors in the ITS: two silicon pixel, two silicon drift, and two silicon strip detectors. The ITS provides high spatial resolution for the position of the primary vertex. The TPC alone is used for momentum and charge determination of particles through the radius of curvature of the particles traversing a 0.5 T longitudinal magnetic field. The TPC additionally provides particle identification through the specific ionization energy loss (dE/dx). To ensure uniform tracking, the z -coordinate (along the beam-axis) of the primary vertex is required to be within a distance of 10 cm from the detector center.

Tracks with a transverse momentum of $0.16 < p_T < 1.0$ GeV/ c and a pseudorapidity of $|\eta| < 0.8$ are retained in this analysis. To ensure good momentum resolution a minimum of 70 tracking points in the TPC are required. The measured energy loss (dE/dx) of particles traversing the TPC and the corresponding uncertainty (σ) are used to select charged pions [28]. Charged tracks observed in the TPC are identified as pions if their dE/dx is within 2σ of the Bethe-Bloch expectation for pions while being more than 2σ away from the Bethe-Bloch expectation for kaons and protons. The pion purity in our sample is studied with the HIJING generator [29], folded with the ALICE acceptance. In the sample selected with the procedure described above, about 96% of the particles are expected to be pions.

The effects of track merging and splitting are minimized by rejecting track pairs whose spatial separation in the TPC is smaller than a threshold value [24]. For three-pion and four-pion correlations, each same-charge pair in the triplet and quadruplet is required to satisfy this condition. Oppositely charged pairs are not required to satisfy this cut as they curve in opposite directions in the solenoidal magnetic field and are therefore easily distinguished.

The low multiplicity events produced in pp and p–Pb collisions contain a non-negligible non-femtoscopic background arising from mini-jets [30–32]. We reduce this background by retaining only high multiplicity events in pp and p–Pb. For pp and p–Pb collisions, we retain events with at least 10 and 15 reconstructed charged pions, respectively. The choice of these boundaries are chosen to provide sufficient statistics while reducing non-femtoscopic background correlations. The multiplicity cut selects events from the top 46% and 42% of the cross-sections, respectively. In Pb–Pb collisions, all non-femtoscopic backgrounds are negligible. We ana-

lyze Pb–Pb data from the top 50% collision centrality in ten equally divided intervals. The collision centrality in Pb–Pb is determined using the charged-particle multiplicity in the V0 detectors [26]. Approximately 13, 52, and 34 million events are used for pp, p–Pb, and Pb–Pb collisions, respectively.

3 Analysis technique

We follow the techniques outlined in Ref. [19] for the extraction of multipion QS correlations and a possible coherent fraction. Several types of multipion correlation functions are presented: C_3^{QS} , c_3^{QS} , C_4^{QS} , a_4^{QS} , b_4^{QS} , and c_4^{QS} . The full three-pion correlation is given by C_3^{QS} and the cumulant correlation is given by c_3^{QS} . Four types of four-pion correlations are defined: the full correlation, C_4^{QS} ; two types of partial cumulant correlations, a_4^{QS} and b_4^{QS} ; and the cumulant correlation, c_4^{QS} .

The full three-pion same-charge correlation function contains both pair and triplet symmetrization sequences while the cumulant contains only the triplet symmetrization sequence. The full four-pion same-charge correlation function contains four sequences of symmetrizations: single-pair, double-pair, triplet, and quadruplet symmetrizations. Partial cumulants, denoted by a_4^{QS} (b_4^{QS}), have single-pair (single- and double-pair) symmetrizations explicitly removed. The cumulant correlation, denoted by c_4^{QS} , represents an isolation of the quadruplet symmetrization sequence.

Two-pion correlations are extracted from two types of pair momentum distributions, $N_1(p_1)N_1(p_2)$ and $N_2(p_1, p_2)$, where p_i is the momentum of particle i . $N_1(p_1)N_1(p_2)$ is measured by sampling two pions from different events with similar characteristic multiplicity and z -coordinate collision vertex class. $N_2(p_1, p_2)$ is measured by sampling both pions from the same event. Three-pion QS correlations are extracted from three types of triplet distributions

$$N_1(p_1)N_1(p_2)N_1(p_3), \quad (1)$$

$$N_2(p_1, p_2)N_1(p_3), \quad (2)$$

$$N_3(p_1, p_2, p_3). \quad (3)$$

Four-pion QS correlations are extracted from the following quadruplet distributions

$$N_1(p_1)N_1(p_2)N_1(p_3)N_1(p_4), \quad (4)$$

$$N_2(p_1, p_2)N_1(p_3)N_1(p_4), \quad (5)$$

$$N_2(p_1, p_2)N_2(p_3, p_4), \quad (6)$$

$$N_3(p_1, p_2, p_3)N_1(p_4), \quad (7)$$

$$N_4(p_1, p_2, p_3, p_4). \quad (8)$$

The distributions in Eqs. 1-8 are formed by sampling the appropriate number of particles from the same event and the rest from different events. The subscript for N represents the number of pions taken from the same event. We normalize the distributions in Eqs. 1-2 to the distribution in Eq. 3 at a suitably large invariant relative momentum, $q_{ij} = \sqrt{-(p_i - p_j)^\mu (p_i - p_j)_\mu}$. Likewise, the distributions in Eqs. 4-7 are normalized to the distribution in Eq. 8. The q_{ij} interval is chosen to be far away from the region of significant QS and FSI correlations. The normalization interval is $0.15 < q_{ij} < 0.2$ GeV/ c in Pb–Pb while being $0.9 < q_{ij} < 1.2$ GeV/ c in pp and p–Pb due to

the wider QS correlations in smaller collision systems. The distributions are all corrected for finite momentum resolution and muon contamination [24].

The two-, three-, and four-pion distributions (N_n^{QS}) are extracted from the measured distributions (N_n) with the appropriate coefficients according to the ‘‘core-halo’’ prescription [33] of short- and long-lived emitters [34]. In the core-halo model, a fraction of particles (f_c) originate within a small radius component of particle production (the core). The rest, $1 - f_c$, originate within a much larger halo radius. The fraction of pairs, triplets, and quadruplets from the core is then given by f_c^2 , f_c^3 , and f_c^4 , respectively. The other possibilities of mixed core-halo compositions are treated as well in this analysis. Pairs of particles from the core of particle production are separated by sufficiently short distances such that their QS and FSI correlations are experimentally observable. Pairs with one or both particles from the halo effectively dilute the correlation functions as no significant QS and FSI correlations are expected. The coefficients that isolate the multipion QS distributions are determined from the f_c parameter [19].

The f_c parameter is often associated with $\sqrt{\lambda}$, where λ parametrizes the correlation strength, which is usually determined from fits to two-particle Bose-Einstein correlations. However, due to the unknown functional form of two-pion correlation functions, the λ parameter, determined this way, is convoluted with the arbitrary choice of fitting functions (e.g. Gaussian fits to non-Gaussian correlation functions). A more accurate extraction of f_c is done by fitting mixed-charge two-pion correlations instead [24]. The correlation between π^+ and π^- is dominated by Coulomb and strong FSI for which the wave functions are well known [35]. Owing to the large pion Bohr radius, $\pi^+\pi^-$ correlations are less sensitive to the detailed structure of the source and can be fit less ambiguously wrt $\pi^+\pi^+$ correlations. As part of the long-lived emitters correspond to weak decays (secondaries), f_c is also sensitive to the specific tracking algorithm’s ability to discriminate primary from secondary tracks. The value, $f_c = 0.84 \pm 0.03$, was used in Ref. [24] as well as in this analysis.

The distinction between core and halo may depend on the characteristic sizes and the dynamics of the system. Pions from decays of mid-lived emitters, such as the K^* , Σ^* , ω , and η' constitute a special case where the effect of QS correlations with other pions can be smaller than that of Coulomb correlations. Therefore, one might expect a slightly smaller core fraction for QS compared to Coulomb interactions. The magnitude of the difference should mainly relate to the fraction of pions produced from decays of mid-lived resonances. The resulting difference, which we assume to be small, is addressed by varying f_c as discussed in the section on systematic uncertainties.

The treatment of multibody FSI (Coulomb and strong) is done according to the generalized Riverside approximation [19, 21, 23, 24, 36] where the n body FSI correlation is treated as the product of each pair FSI correlation,

$$K_3 = K_2(q_{12})K_2(q_{13})K_2(q_{23}), \quad (9)$$

$$K_4 = K_2(q_{12})K_2(q_{13})K_2(q_{14})K_2(q_{23})K_2(q_{24})K_2(q_{34}). \quad (10)$$

The two-pion FSI factor of pair (i, j) is given by $K_2(q_{ij})$ and is calculated by averaging the modulus square of the Coulomb and strong wave function over an assumed freeze-out distribution. We use the THERMINATOR model of particle production as an estimate for the freeze-out distribution [37, 38]. The pair product approach to three-pion FSI correlations was shown to be a good approximation to the full asymptotic wave function calculation [19, 24]. In this article we

present QS correlation functions which are corrected for FSI and for the dilution of long-lived emitters according to Eqs. 33 and 39 in Ref. [19].

All distributions and correlation functions are projected onto the 1D the Lorentz invariant relative momentum. For three- and four-pion correlations, the sum quadrature of pair invariant relative momenta is used:

$$Q_3 = \sqrt{q_{12}^2 + q_{13}^2 + q_{23}^2}, \quad (11)$$

$$Q_4 = \sqrt{q_{12}^2 + q_{13}^2 + q_{14}^2 + q_{23}^2 + q_{24}^2 + q_{34}^2}. \quad (12)$$

The p_T dependence of the correlation functions is studied by further projecting onto the average transverse momenta

$$K_{T2} = \frac{|\vec{p}_{T,1} + \vec{p}_{T,2}|}{2}, \quad (13)$$

$$K_{T3} = \frac{|\vec{p}_{T,1} + \vec{p}_{T,2} + \vec{p}_{T,3}|}{3}, \quad (14)$$

$$K_{T4} = \frac{|\vec{p}_{T,1} + \vec{p}_{T,2} + \vec{p}_{T,3} + \vec{p}_{T,4}|}{4}, \quad (15)$$

for two-, three-, and four-pion correlations, respectively. We form two intervals of K_{T3} defined by $0.16 < K_{T3} < 0.3$ and $0.3 < K_{T3} < 1.0$ GeV/c. Similarly, we define two intervals of K_{T4} as $0.16 < K_{T4} < 0.3$ and $0.3 < K_{T4} < 1.0$ GeV/c. For the low K_{T3} interval which is simultaneously at low Q_3 ($0.02 < Q_3 < 0.03$ GeV/c), $\langle p_T \rangle = 0.23$ GeV/c and the RMS of the p_T distribution is 0.03 GeV/c. At high K_{T3} , $\langle p_T \rangle$ is 0.34 GeV/c and the RMS is 0.03 GeV/c. The same values also closely describe the low and high K_{T4} interval at low Q_4 ($0.045 < Q_4 < 0.06$ GeV/c). We further note that the $\langle p_T \rangle$ is very similar for each q interval in this analysis. For $0.16 < K_{T2} < 0.3$ GeV/c, $\langle p_T \rangle$ increases linearly by about 0.015 GeV/c in the interval $0.005 < q < 0.2$ GeV/c.

3.1 Extracting the pair-exchange magnitudes

The building blocks of Bose-Einstein correlations are the pair-exchange magnitudes (T_{ij}) and the coherent fraction (G) in the absence of multipion phases [5, 18, 19, 39]. Multipion phases are expected when the space-time point of maximum pion emission is momentum dependent. However, the relative momentum dependence of the effect was shown to be rather weak [39]. Assuming a value of G , the pair-exchange magnitudes can be used to build all higher orders of correlation functions. We define the *expected* or *built* correlation functions, $E_n(i)$, which represent the expectation of higher order (n) QS correlations using lower order ($i < n$) experimental measurements as an input. The equations to build E_n are given in appendix A. We define two types of expected correlation functions:

1. $E_3(2)$ and $E_4(2)$: The pair-exchange magnitudes can be extracted directly from two-pion correlation functions, which forms our primary expectation in Pb–Pb collisions. The two-pion correlations are tabulated in four dimensions during the first pass over the data in the longitudinally co-moving system ($q_{\text{out}}, q_{\text{side}}, q_{\text{long}}, K_{T2}$). The interval width of each relative momentum dimension is 5 MeV/c, while it is 50 MeV/c in the K_{T2} dimension. In the second pass over the data, the previously tabulated two-pion correlations are interpolated for each pion pair from mixed events. We interpolate between relative momentum bins with a cubic interpolator. A linear interpolation is used in between K_{T2} bins, where a more linear dependence of correlation strength is observed.

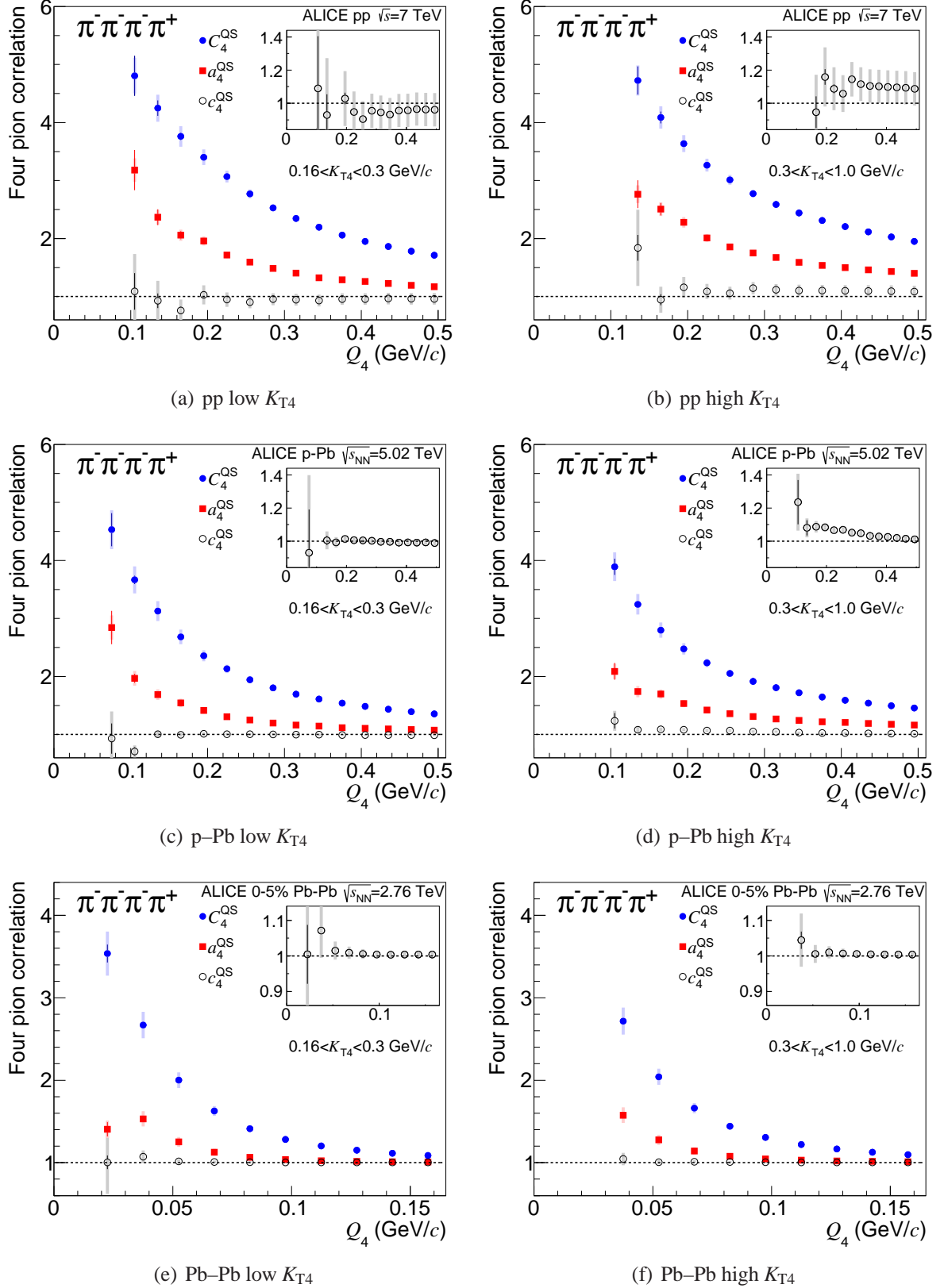


Fig. 1: Mixed-charge ($\pm\pm\pm\mp$) four-pion correlations versus Q_4 in pp, p-Pb, and Pb-Pb. The full (C_4^{QS}), partial cumulant (a_4^{QS}), and cumulant (c_4^{QS}) correlation functions are shown. The inset figure shows a zoom of c_4^{QS} . Systematic uncertainties are shown by the shaded bands. Low and high K_{T4} quadruplets are shown. The average of the charge conjugated correlation functions is shown.

2. $E_4(3)$ and $e_4(3)$: We also extract the pair-exchange magnitudes from fits to C_3^{QS} ($E_4(3)$) and c_3^{QS} ($e_4(3)$) in 3D (q_{12}, q_{13}, q_{23}). The fit is performed according to an Edgeworth parametrization [40] as shown in equation 20 of Ref. [19]. This 2nd approach is more limited as the pair-exchange magnitudes are extracted from a 3D projection of a 9D function. Similar to the 1st type of expected correlations, the pair-exchange magnitudes are obtained from the first pass over the data and input into the second pass.

For the case of partial coherence, we assume that the pair-exchange magnitude of the coherent source is identical to the chaotic one (e.g. same radii) which might be expected for DCC radiation [7]. The value of G may then be extracted by minimizing the χ^2 difference between measured and expected correlations for each Q_3 or Q_4 bin. One may extract G from either of the six same-charge channels: C_4^{QS} , a_4^{QS} , b_4^{QS} , c_4^{QS} , C_3^{QS} , and c_3^{QS} . The primary channel of extraction is C_4^{QS} for reasons of statistical precision and sensitivity to coherent emission. We also extracted G with several other multipion correlations and is shown in a separate note [41]. In pp and p–Pb collisions, where non-negligible non-femtoscopic backgrounds exist, we only use the 2nd build technique as three-pion correlations have a larger signal to background ratio [42].

Both build techniques were tested using data generated by the THERMINATOR model, including a known coherent fraction [19]. The $E_4(2)$ correlations were typically 3% smaller than the “measured correlations” in THERMINATOR. The bias is attributed to the finite 4D projection of the true 6D two-pion correlation function. We correct for this potential bias in a data-driven approach. The interpolated two-pion correlation function from the 4D projection is compared to the true two-pion correlation function for each q interval. The ratio of the two correlation functions (subtracting unity from each), forms our correction factor.

4 Results

We now present the results of three- and four-pion QS correlations in pp, p–Pb, and Pb–Pb collisions. All correlations are corrected for FSI and for the dilution of pions from long-lived emitters. Mixed-charge correlations are first presented to demonstrate the effectiveness of all corrections in the analysis. Fits to same-charge three-pion correlations, which allow us to construct $E_4(3)$ and $e_4(3)$, are then presented. The comparison of measured to expected same-charge correlations assuming the null hypothesis ($G = 0$) is then presented. Finally we present the same comparison with non-zero values of G .

4.1 Mixed-charge four-pion correlation functions

Mixed-charge correlations of the first type ($\pm\pm\pm\mp$) are shown in Figs. 1(a)-1(f). The full correlation contains contributions from two- and three-pion symmetrizations while the partial cumulant (a_4^{QS}) contains only three-pion symmetrizations. The cumulant (c_4^{QS}) has all lower orders ($n < 4$) of symmetrization removed. Its proximity to unity demonstrates the effectiveness of several procedures: the event-mixing technique, FSI corrections, muon corrections, and momentum resolution corrections.

The second type of mixed-charge quadruplets ($\mp\mp\pm\pm$) are shown in Figs. 2(a)-2(f). The full correlation in Figs. 2(a)-2(f) contains contributions from single-pair and double-pair symmetrization sequences. The partial cumulant removes the two-pion symmetrizations while the

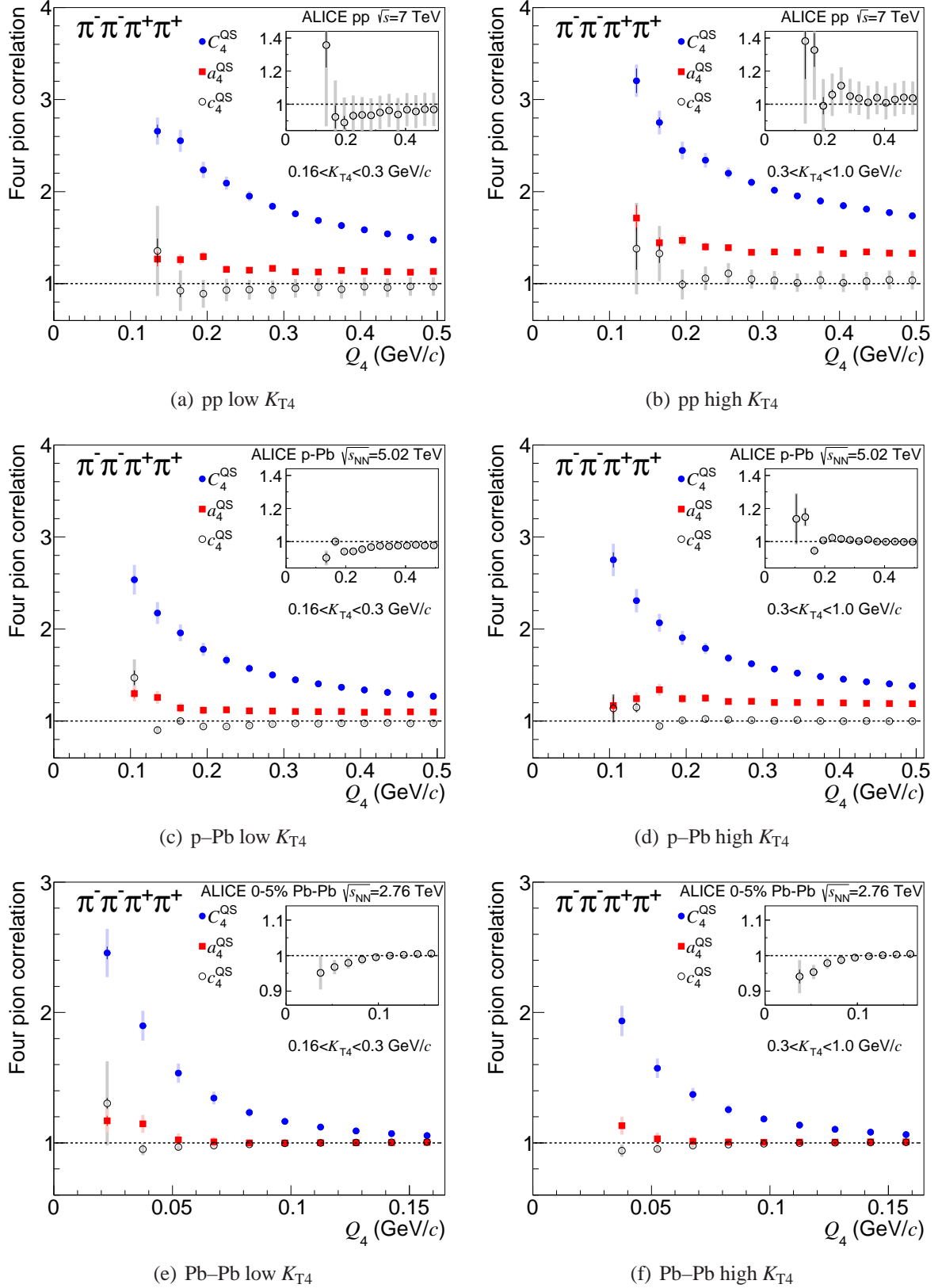


Fig. 2: Mixed-charge ($\mp\mp\pm\pm$) four-pion correlations versus Q_4 in pp, p-Pb, and Pb-Pb. Same details as for Figs. 1(a)-1(f).

cumulant further removes the double-pair symmetrizations. Just as for the first type of mixed-

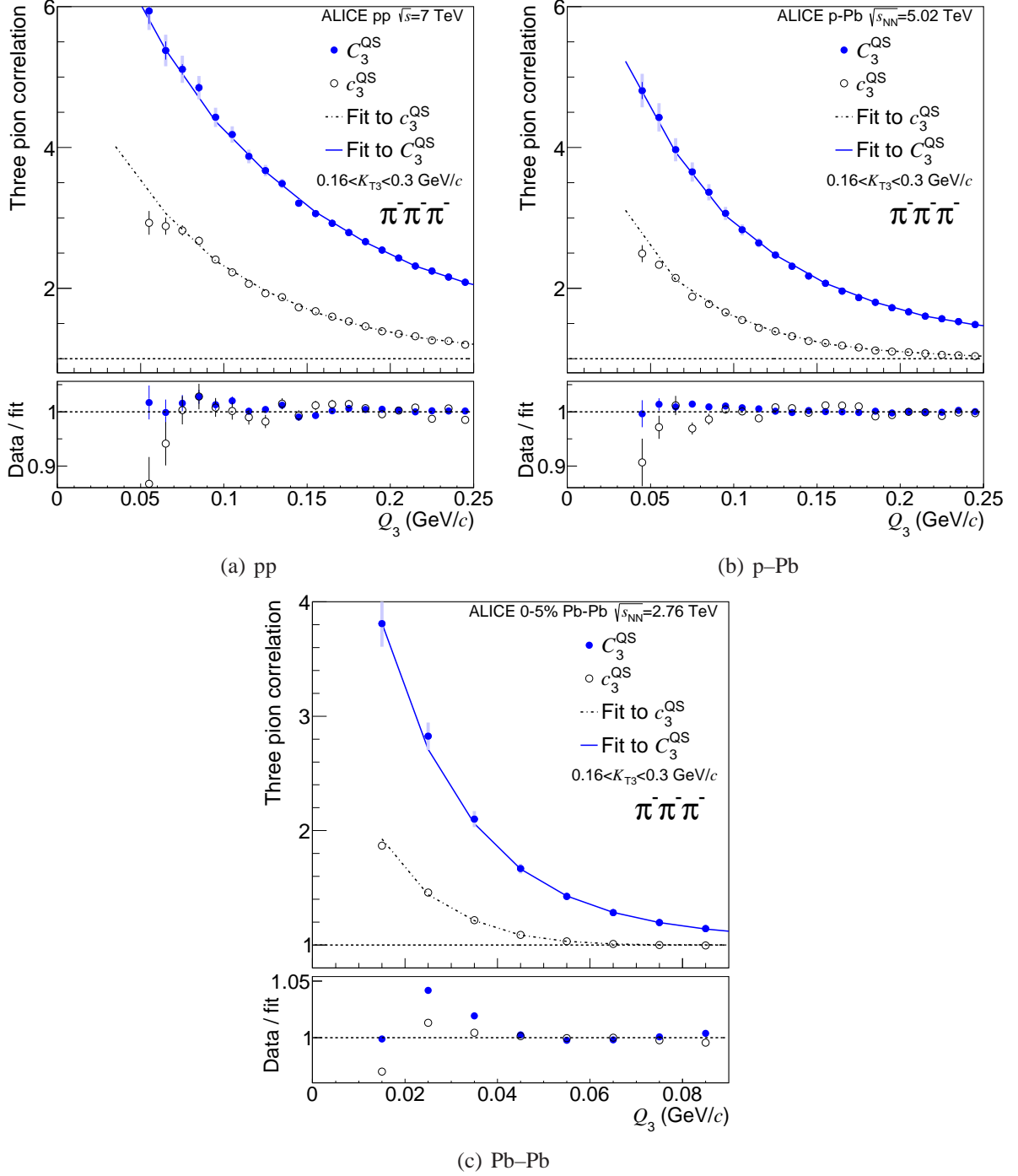


Fig. 3: Same-charge three-pion full and cumulant correlations versus Q_3 with Edgeworth fits in pp, p-Pb, and Pb-Pb collisions. Bottom panels show the ratio of the data to the fit. The fits assume $G = 0$. The systematic uncertainties for C_3^{QS} are given by the shaded band while those for c_3^{QS} are the same after re-scaling by the ratio of correlation strengths. Only statistical errors are shown for the ratio. The average of the charge conjugated correlation functions is shown.

charge quadruplets, the residue seen with the cumulant characterizes the effectiveness of several procedures. The baseline of the cumulant in pp collisions is offset from unity by about 10% and is due to statistical fluctuations in the high q normalization region of our data sample. It is included in the systematic uncertainty. The mixed-charge cumulant residues seen in pp and p-Pb

collisions are similar in magnitude as seen in Pb–Pb collisions. Note that the FSI correlations are larger in pp and p–Pb with respect to Pb–Pb collisions. Isolation of the cumulant correlation function, c_4^{QS} , is done by subtracting several distributions as shown in Eqs. 4-7 after correcting for FSI. By default, we also utilize the distributions of two interacting opposite charge pions, $N_2(-,+)N_1(-)N_1(-)$ and $N_2(-,+)N_1(-)N_1(+)$ for $\pi^-\pi^-\pi^-\pi^+$ and $\pi^-\pi^-\pi^+\pi^+$, respectively. After correcting for finite momentum resolution, muon contamination, and FSI corrections, such distributions should be identical to N_1^4 in the absence of additional correlations. A small difference in c_4^{QS} is observed without the subtraction of such terms [41].

4.1.1 Fits to three-pion correlation functions

The 2nd build technique relies on the extraction of the pair-exchange magnitudes from fits to three-pion correlations. We separately fit both the cumulant (c_3^{QS}) and full (C_3^{QS}) correlations with an Edgeworth parametrization in 3D (q_{12}, q_{13}, q_{23}). The three-pion correlations and fits are projected onto Q_3 for pp, p–Pb, and Pb–Pb collisions in Figs. 3(a)-3(c). The Edgeworth fits have six free parameters, $s, R, \kappa_3, \kappa_4, \kappa_5,$ and κ_6 , [19] as well as a fixed value of G . In Figs. 3(a)-3(c), $G = 0$.

4.2 Same-charge three- and four-pion QS correlations

Figures 4(a)-4(c) present same-charge four-pion correlations in all three collision systems. Each symmetrization sequence is clearly visible. Two different expectations are shown: $E_4(3)$ and $e_4(3)$. The expected correlations in pp and p–Pb are typically within 10% of measured correlations while being closer, 5%, in Pb–Pb.

Three-pion measured and expected correlations in Pb–Pb are presented in Figs. 5(a)-5(b) for low and high K_{T3} . The expected correlations are of the 1st type and assume $G = 0$. The top panels show the full and cumulant three-pion correlations while the bottom panels present the ratio of measured to expected full three-pion correlations. From the bottom panels we observe a Q_3 dependent suppression of measured correlations, compared to the expected correlations.

Four-pion measured correlations are compared to the $E_4(2)$ expectations in Pb–Pb in Figs. 6(a)-6(b) for low and high K_{T4} . Similar to the three-pion case, we observe a Q_4 dependent suppression of measured compared to the expected correlations.

4.3 Extracting a possible coherent fraction

We now investigate the expected correlations with non-zero values of the coherent fraction, G , and compare them to the measured correlations in Pb–Pb. We use the expected correlations of the 1st type to extract the coherent fraction from four-pion correlations. Owing mostly to limitations of the three-pion fitting procedure, we do not extract the coherent fraction with the 2nd type. The isospin effect relevant for charged-particle coherent states is neglected in this analysis [4, 7, 43, 44].

Figure 7 presents same-charge four-pion correlations in Pb–Pb versus Q_4 at low K_{T4} . We observe that the suppression can be partially explained assuming $G = 32\%$ which minimizes the χ^2 of the difference of the ratio from unity for $Q_4 < 0.105$ GeV/ c . The χ^2/DOF of the minimum is quite low, 0.34, and is due to the inclusion of high Q_4 data in the calculation and the rapidly decreasing QS correlation with Q_4 . In Fig. 8 we present same-charge three-pion correlations in Pb–Pb versus Q_3 at low K_{T3} . In contrast to the four-pion case, the value of $G = 32\%$ does not

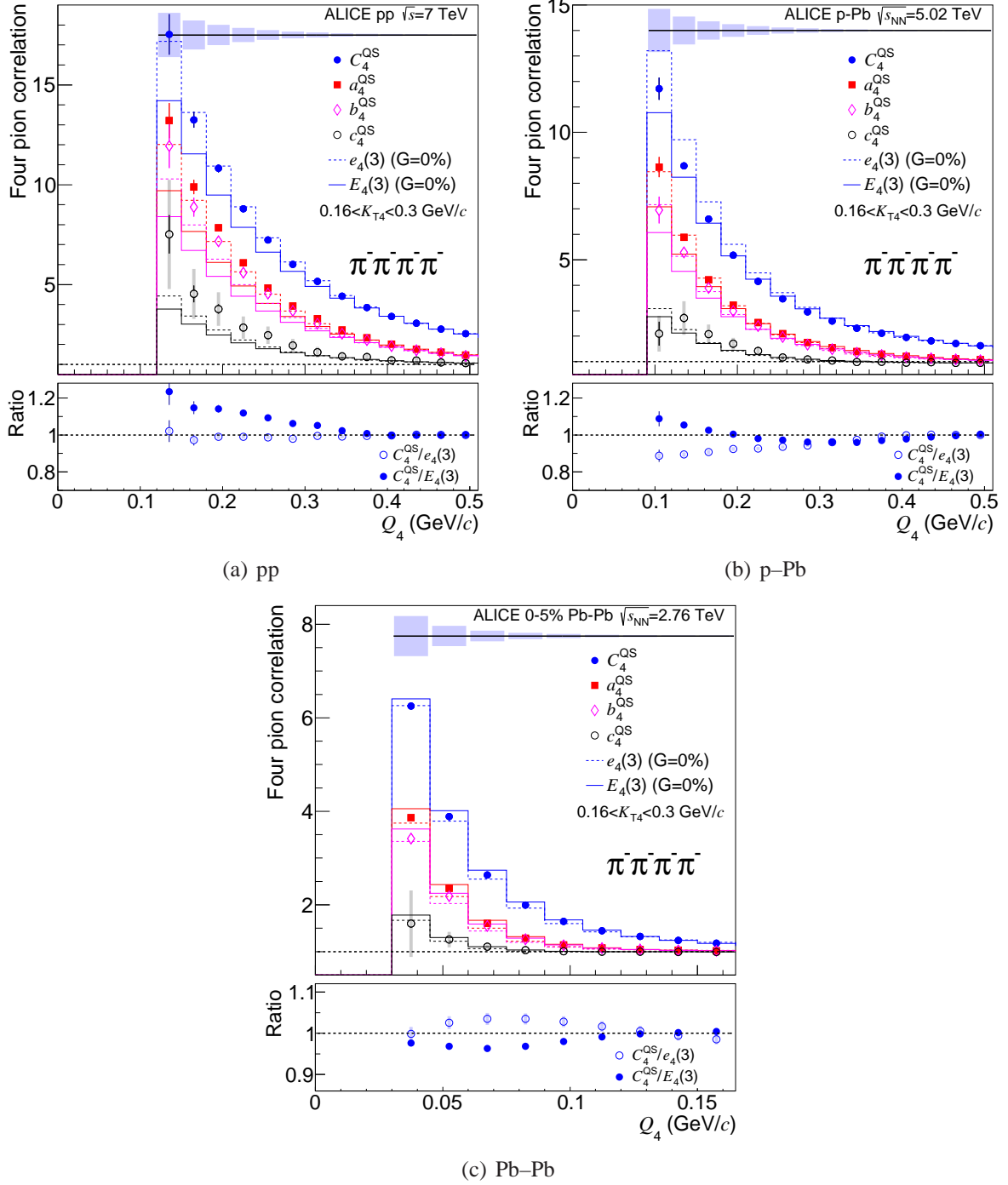


Fig. 4: Same-charge four-pion full (C_4^{QS}), partial cumulant (a_4^{QS} , b_4^{QS}), and cumulant (c_4^{QS}) correlations versus Q_4 in pp (a), p-Pb (b), and Pb-Pb (c) collisions. The solid and dashed block histograms represent $E_4(3)$ and $e_4(3)$ with $G = 0$, respectively. Systematic uncertainties shown at the top apply to C_4^{QS} . The systematics for the other correlation functions are obtained by scaling down the shaded band by the relative correlation strengths. The systematic uncertainties are similar for the expected and measured correlation functions for which the small difference is shown in the ratio. An additional systematic is drawn for c_4^{QS} and is explained in the systematics section. The bottom panel shows the ratio of measured to expected C_4^{QS} . The average of the charge conjugated correlation functions is shown.

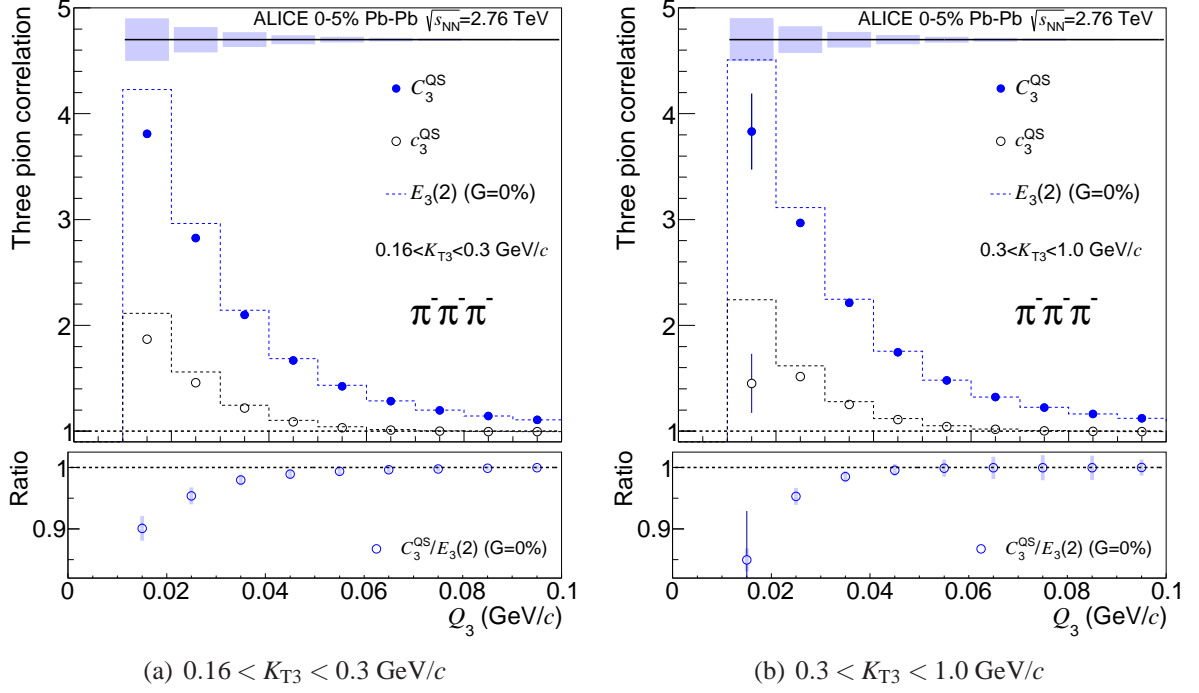


Fig. 5: Three-pion same-charge full (C_3^{QS}) and cumulant (c_3^{QS}) correlations versus Q_3 in Pb–Pb. Expected correlations of the 1st type are shown with dashed block histograms with $G = 0$. The ratio of measured to expected C_3^{QS} is shown in the bottom panel. The systematic uncertainties are shown by the shaded bands at the top of the figure as explained in Fig. 4(a). The average of the charge conjugated correlation functions is shown.

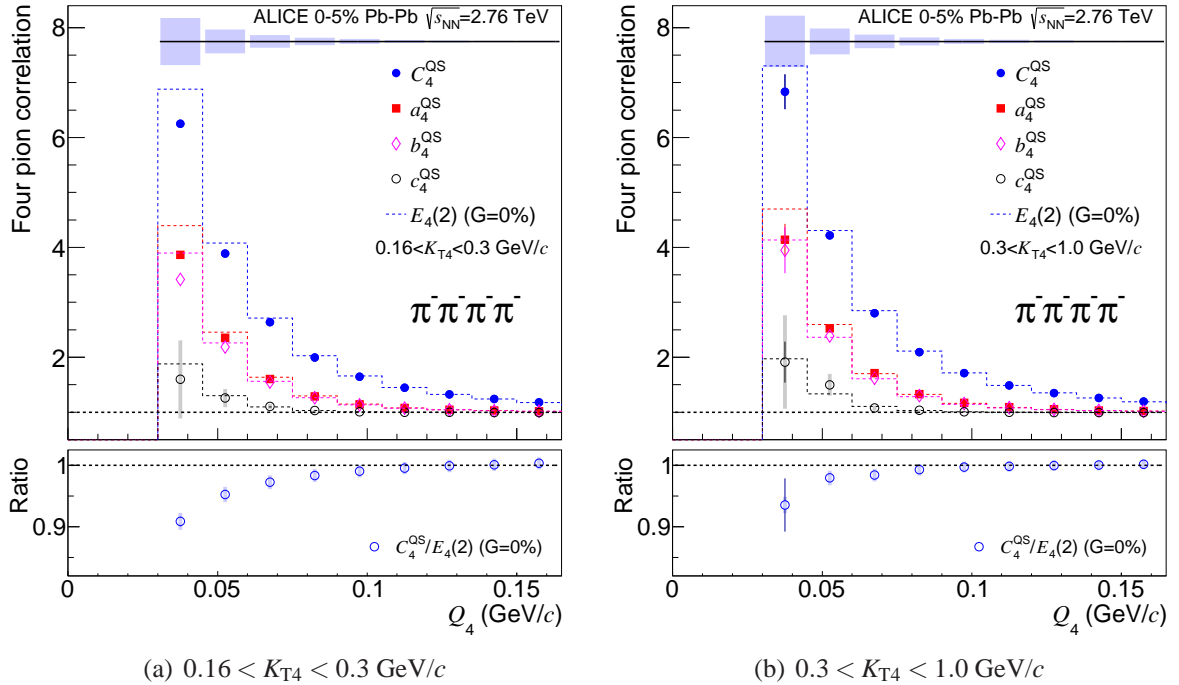


Fig. 6: Four-pion same-charge full and cumulant correlations versus Q_4 in Pb–Pb. Expected correlations of the 1st type are shown with dashed block histograms with $G = 0$. The other details are the same as Fig. 4(a).

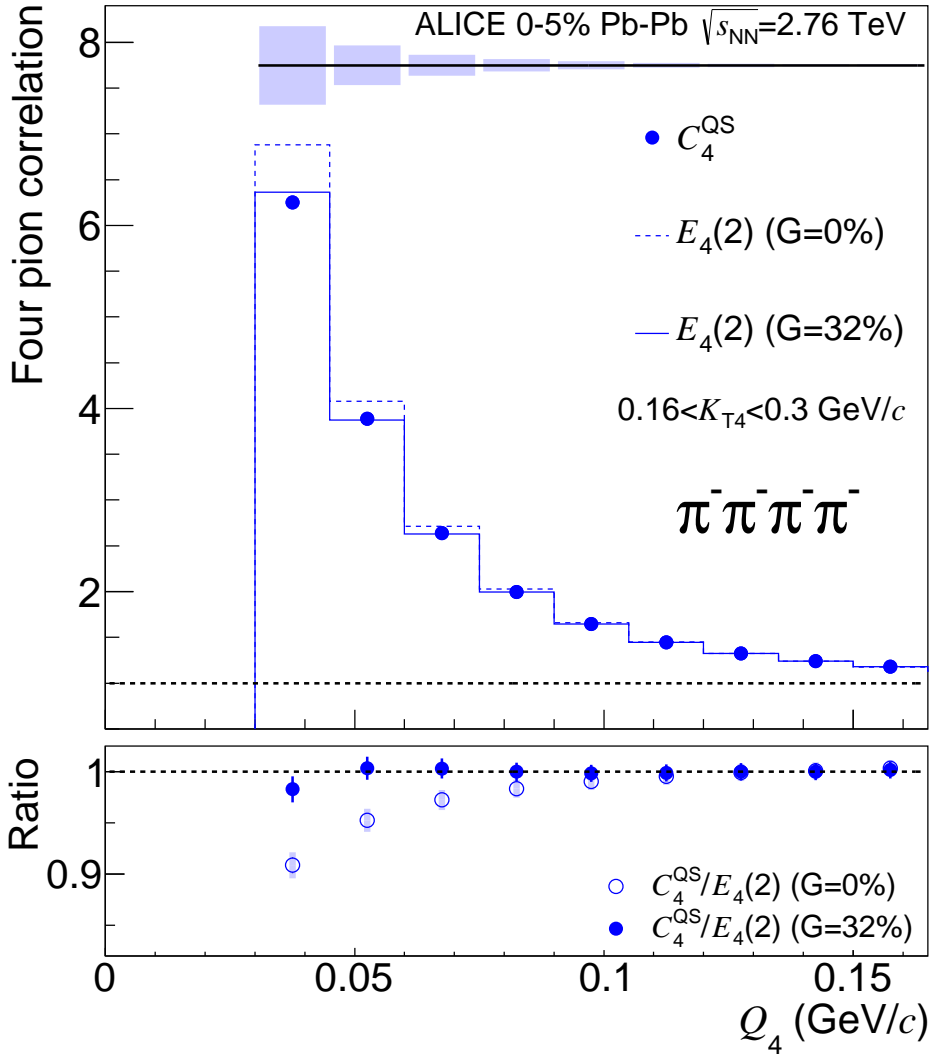


Fig. 7: Same-charge four-pion full (C_4^{QS}) correlations versus Q_4 . Measured and expected correlations of the 1st type are shown. Dashed and solid block histograms show the $G = 0$ and $G = 32\%$ expected correlations, respectively. Systematic uncertainties are shown at the top. The bottom panel shows the ratio of measured to the expected C_4^{QS} . The systematic uncertainties on the ratio are shown with a shaded blue band ($G = 0$) and with a thick blue line ($G = 32\%$).

satisfactorily explain the suppression.

We also studied the centrality dependence of the suppression in Pb–Pb. Figures 9(a) and 9(b) show the centrality dependence of the extracted coherent fraction for low and high K_{T4} . Within statistical and systematic uncertainties, the coherent fractions are consistent for each centrality interval. We also parametrized the coherent component as a point source as opposed to the equal radii assumption used by default. The point source approximation may be expected to be more appropriate for gluon or pion condensate formation. The extracted coherent fractions with the point source approximation are shown in a separate note [41].

Previously [24], the coherent fractions were extracted from the r_3 observable which is intended to isolate the phase of three-pion correlations [39, 45]. In contrast to the previous analysis, we estimate G by averaging the suppression in several Q_3 or Q_4 bins instead of extrapolating r_3 to

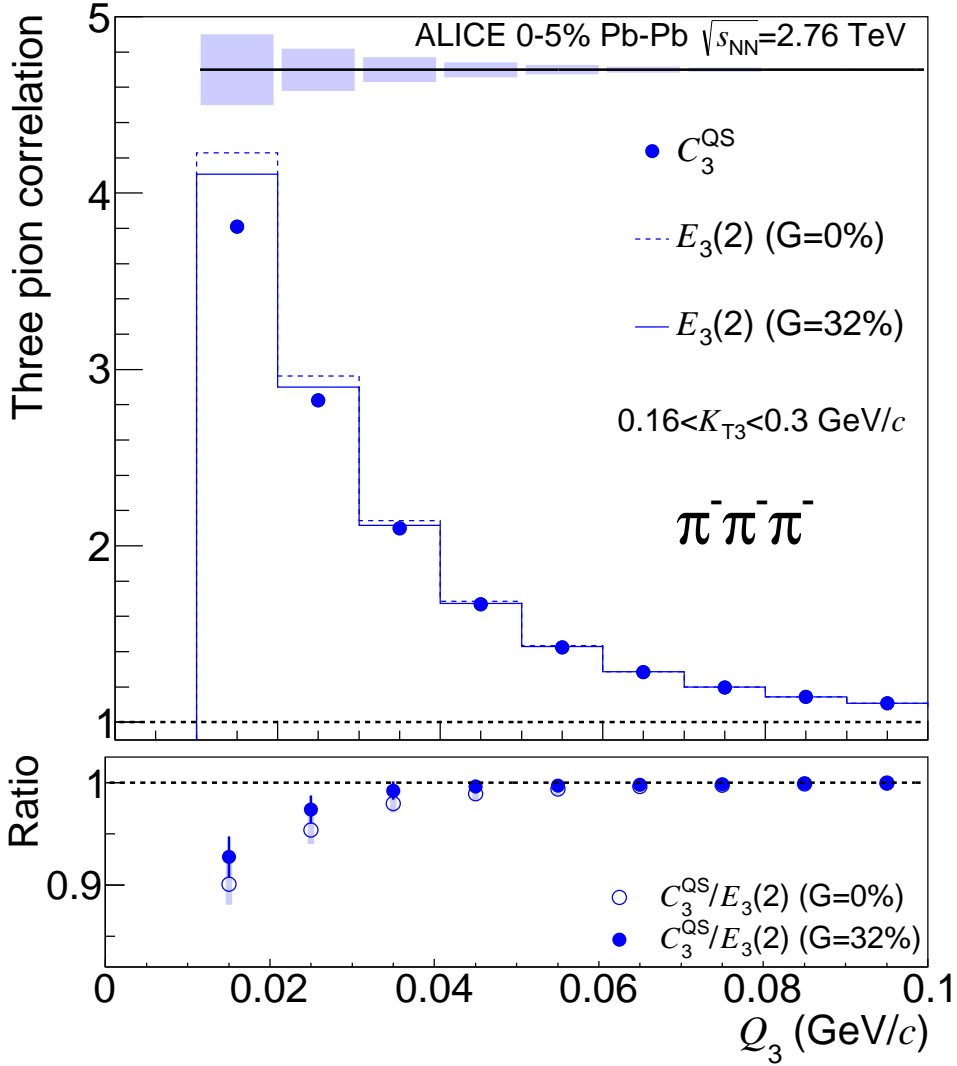


Fig. 8: Same-charge three-pion full (C_3^{QS}) correlations versus Q_3 . Measured and expected correlations of the 1st type are shown. Dashed and solid block histograms show the $G = 0$ and $G = 32\%$ expected correlations, respectively. The other details are the same as in Fig. 7.

the unmeasured intercept. This approach was chosen due to the largely flat relative momentum dependence of previous r_3 measurements [19, 24]. The values of G are obtained by averaging the bin-by-bin values within $0.03 < Q_4 < 0.105$ GeV/ c . Furthermore, our past analysis did not employ interpolation corrections which are relevant for the expected correlations. Correcting for the interpolation biases is expected to lower r_3 [19].

We extracted coherent fractions in Pb–Pb using the expected correlations of the 1st type. The expected correlations of the 2nd type were shown in all three collision systems but are expected to be less accurate due to more limited dimensionality and the fitting procedure of three-pion correlations. Being such, we could not reliably extract a value of G with the 2nd build technique. The 2nd type is, however, preferred in low multiplicity events, where non-negligible background correlations exist.

One of the most commonly cited sources of coherent pion emission is the DCC [8, 10], which may occur as a consequence of chiral symmetry restoration. The most common prediction of

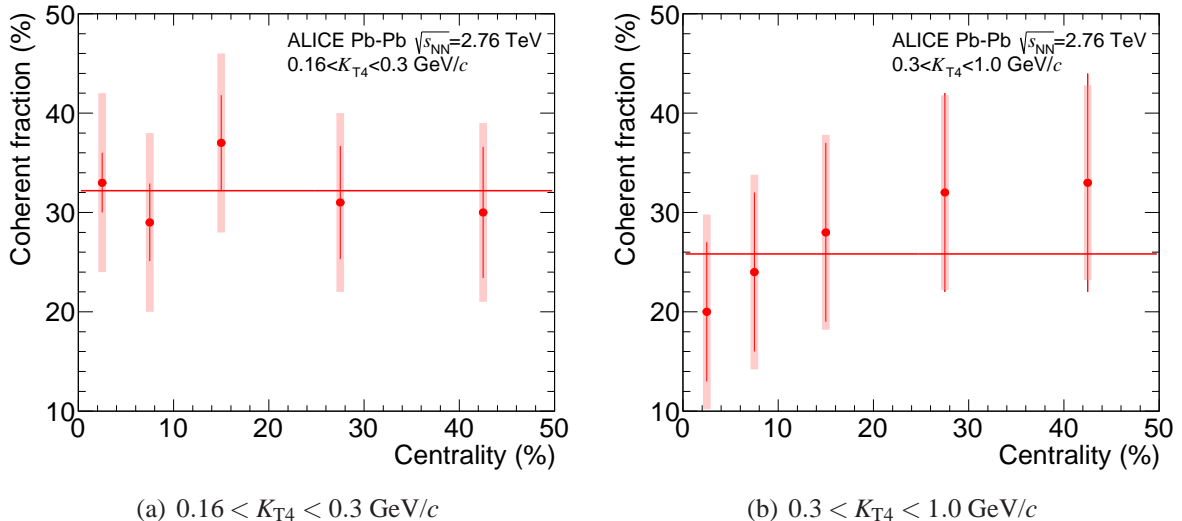


Fig. 9: The extracted coherent fractions (G) from same-charge four-pion correlations versus centrality. Systematic uncertainties are given by the shaded band. A linear fit using only the statistical uncertainties is shown by the horizontal red line.

the DCC is the fluctuation of charged to neutral pion production at low p_T . If a single DCC domain is created within each event, we may expect a surplus of coherent charged pions in one event, while in another event, only coherent neutral pions are present. We investigated this possibility by first isolating a narrow multiplicity class at higher p_T , $0.35 < p_T < 0.5$ GeV/ c , within the 0-5% centrality class determined with the V0 detectors. From the multiplicity distribution of charged pions at the higher p_T interval, we retain events which were within 1 standard deviation from the mean of the distribution. We then analyzed the multiplicity distribution of charged pions at low p_T , $0.16 < p_T < 0.25$ GeV/ c . Events with low p_T multiplicities below the mean of the distribution were stored separately from those events above the mean. We do not observe a significant change of the suppression for events below or above the mean. The finding disfavors single-domain DCCs but does not rule out multidomain DCCs, for which independently coherent charged and neutral pions may be found in a single event [8, 10].

5 Systematic uncertainties

We consider several sources of systematic uncertainty pertaining to the methodology and finite detector resolution. Below we describe each systematic uncertainty studied in order of decreasing magnitude. Some systematic uncertainties apply to only measured or expected correlations while others apply to both. The given values of the uncertainties apply to four-pion correlations. The values for three-pion correlations are generally smaller.

1. f_c scale. The fraction of pion tracks from short-lived emitters for which QS and FSI correlations are experimentally observable is quantified with the f_c parameter. From previous studies in ALICE using fits to $\pi^+\pi^-$ FSI correlations, we estimate that $f_c = 0.84 \pm 0.03$ [24]. We vary f_c within its uncertainties from the previous analysis. The uncertainty derived from varying f_c applies to both measured and expected correlations and is about 6% at low Q_4 . As the uncertainty on f_c given here does not account for the assumption of a universal f_c for both QS and Coulomb correlations (see discussion in Section 3), we have also considered more extreme variations given by $f_c = 0.63$ and $f_c = 0.92$. The

systematic variations of measured and expected correlations are largely correlated. With $f_c = 0.63$, the ratio of measured to expected four-pion correlations increased by about 2% at low Q_4 as compared to the ratio formed with our default $f_c = 0.84$.

2. *FSI variation.* The default two-pion FSI correlation K_2 , together with the default value $f_c = 0.84$, gives a satisfactory description of $\pi^+\pi^-$ correlations [24]. We find that increasing the FSI correlation strength, $|K_2 - 1|$, by 5% while decreasing f_c to 0.806 also provides a satisfactory description of $\pi^+\pi^-$ correlations. The analysis was redone with such modifications, and the ratio of measured to expected four-pion correlations changed by less than 0.5%.
3. *T_{ij} extraction at high q .* The 1st type of expected correlations use the pair-exchange magnitudes (T_{ij}) extracted from two-pion correlations. The extraction of T_{ij} becomes problematic at large q , where the measured two-pion QS correlations fluctuate beneath the baseline due to finite statistics. For such bins we set $T_{ij} = 0$. We also constructed a separate expected correlation where the entire triplet or quadruplet was skipped if any pair T_{ij} was negative. Half of the difference between these two builds was assigned as an uncertainty which is about 4% at high Q_4 and less than 0.1% at low Q_4 .
4. *Interpolation.* We apply a data-driven approach to correct for interpolation biases, as already mentioned. From studies with different interpolation schemes, we find a 1% systematic uncertainty on the expected correlations at low Q_4 .
5. *Mid-lived emitters.* The extraction of the multipion QS correlations from the measured distributions in Eqs. 4-8 relies on the $f_{41}, f_{42}, f_{43}, f_{44}$ coefficients in Ref. [19]. The default values were derived in the ‘‘core-halo’’ picture of particle production, for which there are only short and long-lived emitters. In general there are also mid-lived emitters (e.g. ω decays) which modify the f coefficients and can be estimated using the THERMINATOR model. The effect was found to be quite small [19] and leads to a 0.5% uncertainty at high Q_4 .
6. *Renormalization.* To account for small normalization differences between two-, three-, and four-pion correlation functions, the expected correlations are re-normalized to the ones measured at high Q_4 . In central Pb–Pb, the renormalizations are about 0.9997 ($E_3(2)$), 1.005 ($E_4(2)$), and 1.07 ($e_4(3)$). The interval in Pb–Pb is $0.125 < Q_4 < 0.145$ GeV/ c in central collisions and varies smoothly to $0.165 < Q_4 < 0.185$ GeV/ c in peripheral collisions. The interval in pp and p–Pb is $0.46 < Q_4 < 0.49$ GeV/ c . We take an interval shifted by 15 (60) MeV/ c in Pb–Pb (pp and p–Pb).
7. *Detector resolution.* Numerous effects related to finite detector resolution were checked. The charge conjugated correlation functions were consistent within statistical uncertainties. Similarly, the polarity of the solenoidal magnetic field had a negligible effect on the correlation functions. We compared Pb–Pb data from two different data-taking periods which were known to have different tracking efficiencies. The measured and expected correlation functions differed by less than 0.5%. Finite momentum resolution is known to smear the correlation functions, decreasing the correlation strength at low relative momentum for all orders of correlation functions. We correct for finite momentum resolution using HIJING (Pb–Pb) and PYTHIA[46] (pp and p–Pb) data simulated with the ALICE detector response. The uncertainty on the momentum resolution at low p_T is governed

by the material budget uncertainty of the ALICE detector and is estimated to be less than 10%. The corresponding uncertainty on the measured and expected correlations is about 1%. Our pion purity is estimated to be about 96% for which the remaining 4% impurity is dominated by muon contamination. Simulations have shown that most of the muons in our sample originate from charged pion decays for which QS and FSI correlations are expected with primary pions. We apply muon corrections similar to Refs. [24, 42]. We assign a 2% uncertainty to the muon correction procedure. The tracking efficiency of the ALICE detector decreases rapidly for $p_T < 0.2$ GeV/ c [28]. To estimate the potential bias caused by the tracking efficiency, we randomly discard pions in THERMINATOR according to the TPC reconstruction efficiency. We do not observe a bias on the measured nor expected correlation functions which could cause an artificial suppression.

In addition to the above mentioned sources of systematics, we also applied an additional uncertainty to cumulant correlation functions, c_4^{QS} . The cumulant correlations were found to be much more sensitive to effects induced by low statistics at low Q_4 . The additional uncertainty is several tens of percents for the lowest Q_4 bin.

Most of the systematic uncertainties were found to be similar in magnitude and highly correlated for both measured and expected correlations. As a consequence, the systematics largely cancel in the ratio of measured to expected. For the ratio, we apply the maximum difference of measured and expected systematics. The systematic uncertainties for the ratio are dominated by the interpolator and mid-lived emitter uncertainty at low Q_4 . At high Q_4 , the muon corrections and the extraction of T_{ij} at high q dominate the uncertainties.

6 Possible origins of the suppression

A suppression of three- and four-pion Bose-Einstein correlations compared to the expectations from two-pion measurements has been observed in Pb–Pb collisions. Below we list our investigations into the origin of the suppression.

1. *Quantum coherence.* Incorporating the effects of quantum coherence can perhaps explain the four-pion suppression in Fig. 7 with a centrality averaged coherent fraction of $32\% \pm 3\%$ (stat) $\pm 9\%$ (syst). However, the same coherent fraction fails to explain the suppression at the three-pion level in Fig. 8. In particular, the suppression at the lowest Q_3 and Q_4 intervals cannot be resolved with the same coherent fraction as needed at higher Q_3 and Q_4 intervals. The isospin effect for charged-pion coherent states [4, 7, 43, 44] has not been calculated, since the expressions which incorporate isospin conservation do not exist at the four-pion level. For $G = 32\%$, the isospin effect increases the intercept of two- and three-pion correlations by about 1% and 3%, respectively. The effect on the expected correlations at finite relative momentum has not been calculated.
2. *Coulomb repulsion.* Same-charge pions experience Coulomb and strong repulsion which is stronger for quadruplets than for pairs. The four-pion Coulomb corrections used in this analysis correspond to the asymptotic limit of the Coulomb wave function as mentioned before. Previous studies [47] have justified the use of such wave functions for the characteristic freeze-out volumes and relative momenta studied in this analysis. We have also shown that the cumulant (c_4^{QS}) of mixed-charge correlations are near unity after FSI

	--+	+++	----+	--++	++++
Low K_{T3}, K_{T4}	1.07 ± 0.01	1.16 ± 0.02	1.6 ± 0.1	0.89 ± 0.02	1.17 ± 0.02
High K_{T3}, K_{T4}	1.06 ± 0.01	1.13 ± 0.02	1.2 ± 0.1	0.89 ± 0.02	1.09 ± 0.02

Table 1: The x factors used to modify the multipion FSI factor such that the suppression of same-charge correlations and the residues of mixed-charged cumulants are resolved. The multipion FSI factor is modified according to: $K_{3,4} \rightarrow x|K_{3,4} - 1| + 1$. With ----+ correlations, only K_4 was modified and not K_3 which is also used to isolate the cumulant. We further note that x is more Q_3 and Q_4 dependent for the case of +++ and +++. We find that for the lowest Q_3 and Q_4 bin, x is about 1.2.

corrections. In the case that the genuine multipion Coulomb interactions are not negligible, we modify the three- and four-pion FSI correlations by an amount, x , needed to resolve the suppression (residue) of same-charge (mixed-charge) correlations. The FSI factors are modified as: $K_{3,4} \rightarrow x|K_{3,4} - 1| + 1$. The x factors given in Tab. 1 demonstrate that if the suppression is solely caused by genuine multipion Coulomb effects, they should modify the two-body approximation by up to 20% at low relative momentum for the case of same-charge three- and four-pion correlations. Such large multibody Coulomb correlations are not expected from the arguments provided in Ref. [47].

3. *Mid-lived emitters.* Uncertainties of mid-lived resonance production ($\Gamma \sim 10$ MeV) result in uncertainties of f_{44} , f_{43} , f_{42} , and f_{41} [19] which are used to isolate the QS correlations from the measured distributions. We investigated the possibility of decreasing f_{44} while equally increasing f_{41} , $6f_{42}$, and $4f_{43}$ following the unitary probability constraint: $f_{44} + 4f_{43} + 6f_{42} + f_{41} = 1$. Decreasing f_{44} by 0.08 resolves the suppression for $Q_4 < 0.06$ while 0.04 is more appropriate for larger Q_4 . However, as a consequence the ----+ and --++ cumulant correlations increase by as much as 0.2 at low Q_4 , which leaves larger unexplained residues.
4. *Background correlations.* Event generators such as HIJING and AMPT [48] do not include the effects of QS nor FSI and may thus be used to estimate background correlations. We checked two-, three-, and four-pion correlation functions in the 5% most central events from HIJING and AMPT. All orders of correlation functions were consistent with unity.
5. *Multipion phases.* The expected correlations ignore the three- and four-pion Fourier transform phases [39]. The r_3 observable was extracted in ALICE [24] and THERMINATOR [19] and no significant Q_3 dependence was found. As the trend of G with Q_3 and Q_4 is opposite to that expected from the phases [41], we find them unlikely to explain the suppression.
6. *Multipion distortions.* At high freeze-out phase-space density, all higher order symmetrizations, which are usually neglected, can contribute significantly to all orders of correlation functions [49–53]. The distortions have been calculated for two-pion correlations and recently for three- and four-pion correlations [19]. The calculations suggest that the ratio of measured to expected correlations is robust with respect to this effect.

7 Summary

Three- and four-pion QS correlations have been measured in pp, p–Pb, and Pb–Pb collisions at the LHC. The measured same-charge multipion correlations are compared to the expectation from lower order experimental correlation functions. A significant suppression of multipion Bose-Einstein correlations has been observed in Pb–Pb collisions. The ratio of measured to expected same-charge four-pion correlations is about 6σ below unity in our lowest Q_4 interval.

In pp and p–Pb collisions, owing to background correlations at low multiplicity in two-pion correlation functions, we compare the measured four-pion correlations to the expectation from fits to three-pion correlations ($E_4(3)$ and $e_4(3)$). Three-pion correlation functions contain substantially larger QS correlations and reduced background correlations, which makes them a preferred base for higher order expectations in pp and p–Pb collisions. We do not observe a significant suppression of four-pion correlations in pp nor p–Pb collisions. However, the more limited dimensionality and fitting procedure to three-pion correlations makes $E_4(3)$ and $e_4(3)$ expectations less accurate than $E_4(2)$. Nevertheless, despite the presence of the non-femtoscopic background, we also performed the analysis in pp and p–Pb collisions with the first type of expected correlations ($E_4(2)$ and $E_3(2)$). No significant suppression was observed in pp or p–Pb collisions, although the unknown strength of the non-femtoscopic background prevents an absolute statement.

Mixed-charge four-pion correlations have also been measured. They are used to demonstrate the effectiveness of the cumulant isolation via the event-mixing techniques as well as that of the FSI, muon, and momentum resolution corrections. The mixed-charge cumulant correlations are shown to be near unity although a finite residue exists with both types of mixed-charge correlations.

The suppression of same-charge three- and four-pion correlations in Fig. 7 and 8 cannot be unambiguously resolved with any of the possible origins discussed. For example, if genuine multipion Coulomb interactions are non negligible, a large increase of as much as 20% beyond the two-body approximation would be needed to account for the observed suppression. On the other hand, a coherent fraction of about $32\% \pm 3\%(\text{stat}) \pm 9\%(\text{syst})$ could largely explain the four-pion suppression, but the same value cannot explain the three-pion suppression. There does not appear to be a significant centrality dependence to the extracted coherent fractions. The weak K_{T2} dependence of the coherent fractions does not favor the formation of Bose-Einstein condensates nor disoriented chiral condensates, which are expected to radiate mostly at low p_T . The suppression observed in this analysis appears to extend at least up to $p_T \sim 340 \text{ MeV}/c$.

Acknowledgements

We would like to thank Richard Lednický and Tamás Csörgő for numerous helpful discussions.

The ALICE Collaboration would like to thank all its engineers and technicians for their invaluable contributions to the construction of the experiment and the CERN accelerator teams for the outstanding performance of the LHC complex. The ALICE Collaboration gratefully acknowledges the resources and support provided by all Grid centres and the Worldwide LHC Computing Grid (WLCG) collaboration. The ALICE Collaboration acknowledges the following funding agencies for their support in building and running the ALICE detector: State Committee of Science, World Federation of Scientists (WFS) and Swiss Fonds Kidagan,

Armenia; Conselho Nacional de Desenvolvimento Científico e Tecnológico (CNPq), Financiadora de Estudos e Projetos (FINEP), Fundação de Amparo à Pesquisa do Estado de São Paulo (FAPESP); National Natural Science Foundation of China (NSFC), the Chinese Ministry of Education (CMOE) and the Ministry of Science and Technology of China (MSTC); Ministry of Education and Youth of the Czech Republic; Danish Natural Science Research Council, the Carlsberg Foundation and the Danish National Research Foundation; The European Research Council under the European Community's Seventh Framework Programme; Helsinki Institute of Physics and the Academy of Finland; French CNRS-IN2P3, the 'Region Pays de Loire', 'Region Alsace', 'Region Auvergne' and CEA, France; German Bundesministerium für Bildung, Wissenschaft, Forschung und Technologie (BMBF) and the Helmholtz Association; General Secretariat for Research and Technology, Ministry of Development, Greece; National Research, Development and Innovation Office (NKFIH), Hungary; Department of Atomic Energy and Department of Science and Technology of the Government of India; Istituto Nazionale di Fisica Nucleare (INFN) and Centro Fermi - Museo Storico della Fisica e Centro Studi e Ricerche "Enrico Fermi", Italy; Japan Society for the Promotion of Science (JSPS) KAKENHI and MEXT, Japan; Joint Institute for Nuclear Research, Dubna; National Research Foundation of Korea (NRF); Consejo Nacional de Ciencia y Tecnología (CONACYT), Dirección General de Asuntos del Personal Académico (DGAPA), México, Amérique Latine Formation académique - European Commission (ALFA-EC) and the EPLANET Program (European Particle Physics Latin American Network); Stichting voor Fundamenteel Onderzoek der Materie (FOM) and the Nederlandse Organisatie voor Wetenschappelijk Onderzoek (NWO), Netherlands; Research Council of Norway (NFR); National Science Centre, Poland; Ministry of National Education/Institute for Atomic Physics and National Council of Scientific Research in Higher Education (CNCSI-UEFISCDI), Romania; Ministry of Education and Science of Russian Federation, Russian Academy of Sciences, Russian Federal Agency of Atomic Energy, Russian Federal Agency for Science and Innovations and The Russian Foundation for Basic Research; Ministry of Education of Slovakia; Department of Science and Technology, South Africa; Centro de Investigaciones Energéticas, Medioambientales y Tecnológicas (CIEMAT), E-Infrastructure shared between Europe and Latin America (EELA), Ministerio de Economía y Competitividad (MINECO) of Spain, Xunta de Galicia (Consellería de Educación), Centro de Aplicaciones Tecnológicas y Desarrollo Nuclear (CEADEN), Cubaenergía, Cuba, and IAEA (International Atomic Energy Agency); Swedish Research Council (VR) and Knut & Alice Wallenberg Foundation (KAW); Ukraine Ministry of Education and Science; United Kingdom Science and Technology Facilities Council (STFC); The United States Department of Energy, the United States National Science Foundation, the State of Texas, and the State of Ohio; Ministry of Science, Education and Sports of Croatia and Unity through Knowledge Fund, Croatia; Council of Scientific and Industrial Research (CSIR), New Delhi, India; Pontificia Universidad Católica del Perú.

References

- [1] R. H. Brown and R. Q. Twiss, "Correlation between Photons in two Coherent Beams of Light," *Nature* **177** (1956) 27–29.
- [2] G. Goldhaber, S. Goldhaber, W.-Y. Lee, and A. Pais, "Influence of Bose-Einstein statistics on the anti-proton proton annihilation process," *Phys.Rev.* **120** (1960) 300–312.

- [3] G. Kopylov and M. Podgoretsky, “The interference of two-particle states in particle physics and astronomy,” *Zh.Eksp.Teor.Fiz.* **69** (1975) 414–421.
- [4] M. Gyulassy, S. Kauffmann, and L. Wilson, “Pion Interferometry of Nuclear Collisions. 1. Theory,” *Phys.Rev.* **C20** (1979) 2267–2292.
- [5] I. Andreev, M. Plumer, and R. Weiner, “Quantum statistical approach to Bose-Einstein correlations and its experimental implications,” *Int.J.Mod.Phys.* **A8** (1993) 4577–4626.
- [6] M. Plumer, L. Razumov, and R. Weiner, “Evidence for quantum statistical coherence from experimental data on higher order Bose-Einstein correlations,” *Phys.Lett.* **B286** (1992) 335–340.
- [7] S. Akkelin, R. Lednicky, and Y. Sinyukov, “Correlation search for coherent pion emission in heavy ion collisions,” *Phys.Rev.* **C65** (2002) 064904, arXiv:0107015 [nucl-th].
- [8] J. Bjorken, K. Kowalski, and C. Taylor, “Baked Alaska,” SLAC-PUB-6109, C93-03-07.
- [9] C. Greiner, C. Gong, and B. Muller, “Some remarks on pion condensation in relativistic heavy ion collisions,” *Phys. Lett.* **B316** (1993) 226–230, arXiv:hep-ph/9307336 [hep-ph].
- [10] J. Bjorken, “Disoriented chiral condensate: Theory and phenomenology,” *Acta Phys.Polon.* **B28** (1997) 2773–2791, arXiv:hep-ph/9712434 [hep-ph].
- [11] K. Rajagopal, “Disorienting the chiral condensate at the QCD phase transition,” arXiv:hep-ph/9703258 [hep-ph].
- [12] U. Ornik, M. Plumer, and D. Strottman, “Bose condensation through resonance decay,” *Phys.Lett.* **B314** (1993) 401–407.
- [13] J.-P. Blaizot, F. Gelis, J.-F. Liao, L. McLerran, and R. Venugopalan, “Bose-Einstein Condensation and Thermalization of the Quark Gluon Plasma,” *Nucl.Phys.* **A873** (2012) 68–80, arXiv:1107.5296 [hep-ph].
- [14] J.-P. Blaizot, F. Gelis, J. Liao, L. McLerran, and R. Venugopalan, “Thermalization and Bose-Einstein Condensation in Overpopulated Glasma,” *Nucl.Phys.* **A904-905** (2013) 829c–832c, arXiv:1210.6838 [hep-ph].
- [15] V. Begun and W. Florkowski, “Bose-Einstein condensation of pions in heavy-ion collisions at the CERN Large Hadron Collider (LHC) energies,” *Phys. Rev.* **C91** (2015) 054909, arXiv:1503.04040 [nucl-th].
- [16] E. Ikonen, “Chaoticity parameter lambda and multiple coherent components in relativistic heavy-ion collisions,” *Phys.Rev.* **C78** (2008) 051901.
- [17] **UA1-Minimum Bias-Collaboration** Collaboration, N. Neumeister *et al.*, “Higher order Bose-Einstein correlations in $p\bar{p}$ collisions at $\sqrt{s} = 630$ and 900 GeV,” *Phys.Lett.* **B275** (1992) 186–194.
- [18] T. Csorgo, “Particle interferometry from 40-MeV to 40-TeV,” *Heavy Ion Phys.* **15** (2002) 1–80, arXiv:hep-ph/0001233 [hep-ph].

- [19] D. Gangadharan, “Techniques for multiboson interferometry,” *Phys. Rev.* **C92** no. 1, (2015) 014902, arXiv:1502.02121 [nucl-th].
- [20] NA44 Collaboration, H. Boggild *et al.*, “Three pion correlations in sulphur lead collisions at the CERN SPS,” *Phys.Lett.* **B455** (1999) 77–83.
- [21] WA98 Collaboration, M. Aggarwal *et al.*, “Three pion interferometry results from central Pb–Pb collisions at 158-A-GeV/c,” *Phys.Rev.Lett.* **85** (2000) 2895, arXiv:0008018 [hep-ex].
- [22] NA44 Collaboration, I. Bearden *et al.*, “One-dimensional and two-dimensional analysis of 3π correlations measured in Pb–Pb interactions,” *Phys.Lett.* **B517** (2001) 25–31, arXiv:0102013 [nucl-ex].
- [23] STAR Collaboration, J. Adams *et al.*, “Three pion HBT correlations in relativistic heavy ion collisions from the STAR experiment,” *Phys.Rev.Lett.* **91** (2003) 262301, arXiv:0306028 [nucl-ex].
- [24] ALICE Collaboration, B. Abelev *et al.*, “Two and Three-Pion Quantum Statistics Correlations in Pb–Pb Collisions at $\sqrt{s_{NN}}=2.76$ TeV at the LHC,” *Phys.Rev.* **C89** (2014) 024911, arXiv:1310.7808 [nucl-ex].
- [25] ALICE Collaboration, K. Aamodt *et al.*, “The ALICE experiment at the CERN LHC,” *JINST* **3** (2008) S08002.
- [26] ALICE Collaboration, B. Abelev *et al.*, “Centrality determination of Pb–Pb collisions at $\sqrt{s_{NN}} = 2.76$ TeV with ALICE,” *Phys.Rev.* **C88** (2013) 044909, arXiv:1301.4361 [nucl-ex].
- [27] J. Alme, Y. Andres, H. Appelshauser, S. Bablok, N. Bialas, *et al.*, “The ALICE TPC, a large 3-dimensional tracking device with fast readout for ultra-high multiplicity events,” *Nucl.Instrum.Meth.* **A622** (2010) 316–367, arXiv:1001.1950 [physics.ins-det].
- [28] ALICE Collaboration, B. Abelev *et al.*, “Performance of the ALICE Experiment at the CERN LHC,” *Int. J. Mod. Phys.* **A29** (2014) 1430044, arXiv:1402.4476 [nucl-ex].
- [29] X.-N. Wang and M. Gyulassy, “HIJING: A Monte Carlo model for multiple jet production in pp, pA and AA collisions,” *Phys.Rev.* **D44** (1991) 3501–3516.
- [30] ALICE Collaboration, K. Aamodt *et al.*, “Two-pion Bose-Einstein correlations in pp collisions at $\sqrt{s} = 900$ GeV,” *Phys.Rev.* **D82** (2010) 052001, arXiv:1007.0516 [hep-ex].
- [31] ALICE Collaboration, K. Aamodt *et al.*, “Femtoscopy of pp collisions at $\sqrt{s} = 0.9$ and 7 TeV at the LHC with two-pion Bose-Einstein correlations,” *Phys.Rev.* **D84** (2011) 112004, arXiv:1101.3665 [hep-ex].
- [32] ALICE Collaboration, J. Adam *et al.*, “Two-pion femtoscopy in p–Pb collisions at $\sqrt{s_{NN}} = 5.02$ TeV,” *Phys. Rev.* **C91** (2015) 034906, arXiv:1502.00559 [nucl-ex].
- [33] T. Csorgo, B. Lorstad, and J. Zimanyi, “Bose-Einstein correlations for systems with large halo,” *Z.Phys.* **C71** (1996) 491–497, arXiv:hep-ph/9411307 [hep-ph].

- [34] R. Lednicky and M. Podgoretsky, “The interference of identical particles emitted by sources of different sizes,” *Sov.J.Nucl.Phys.* **30** (1979) 432.
- [35] R. Lednicky, “Finite-size effects on two-particle production in continuous and discrete spectrum,” *Phys.Part.Nucl.* **40** (2009) 307–352, arXiv:0501065 [nucl-th].
- [36] Y. Liu, D. Beavis, S. Chu, S. Fung, D. Keane, *et al.*, “Three Pion Correlations in Relativistic Heavy Ion Collisions,” *Phys.Rev.* **C34** (1986) 1667–1672.
- [37] A. Kisiel, T. Taluc, W. Broniowski, and W. Florkowski, “THERMINATOR: THERMal heavy-IoN generATOR,” *Comput.Phys.Commun.* **174** (2006) 669–687, arXiv:0504047 [nucl-th].
- [38] M. Chojnacki, A. Kisiel, W. Florkowski, and W. Broniowski, “THERMINATOR 2: THERMal heavy IoN generATOR 2,” *Comput.Phys.Commun.* **183** (2012) 746–773, arXiv:1102.0273 [nucl-th].
- [39] U. W. Heinz and Q. Zhang, “What can we learn from three pion interferometry?,” *Phys.Rev.* **C56** (1997) 426–431, arXiv:9701023 [nucl-th].
- [40] T. Csorgo and S. Hegyi, “Model independent shape analysis of correlations in 1, 2 or 3 dimensions,” *Phys.Lett.* **B489** (2000) 15–23.
- [41] ALICE Collaboration, J. Adam *et al.*, “Supplemental figures: Multipion Bose-Einstein correlations in pp, p-Pb and Pb-Pb collisions at the LHC,” *ALICE-PUBLIC-2015-009* (2015).
- [42] ALICE Collaboration, B. Abelev *et al.*, “Freeze-out radii extracted from three-pion cumulants in pp, p-Pb and Pb-Pb collisions at the LHC,” *Phys.Lett.* **B739** (2014) 139–151, arXiv:1404.1194 [nucl-ex].
- [43] J. C. Botke, D. J. Scalapino, and R. L. Sugar, “Coherent states and particle production,” *Phys. Rev.* **D9** (1974) 813–823.
- [44] M. Biyajima, A. Ohsawa, N. Suzuki, and I. V. Andreev, “Isotopic spin effect in two pion and three pion Bose-Einstein correlations,” *Phys. Rev.* **C58** (1998) 2316–2320.
- [45] U. W. Heinz and A. Sugarbaker, “Projected three-pion correlation functions,” *Phys.Rev.* **C70** (2004) 054908, arXiv:0408056 [nucl-th].
- [46] T. Sjostrand, S. Mrenna, and P. Z. Skands, “PYTHIA 6.4 Physics and Manual,” *JHEP* **0605** (2006) 026, arXiv:hep-ph/0603175 [hep-ph].
- [47] E. Alt, T. Csorgo, B. Lorstad, and J. Schmidt-Sorensen, “Coulomb corrections to the three-body correlation function in high-energy heavy-ion reactions,” *Phys.Lett.* **B458** (1999) 407–414, arXiv:hep-ph/9812474 [hep-ph].
- [48] Z.-W. Lin, C. M. Ko, B.-A. Li, B. Zhang, and S. Pal, “A Multi-phase transport model for relativistic heavy-ion collisions,” *Phys.Rev.* **C72** (2005) 064901, arXiv:0411110 [nucl-th].

- [49] W. A. Zajc, “Monte Carlo Computational Methods for the Generation of Events with Bose-Einstein Correlations,” *Phys.Rev.* **D35** (1987) 3396.
- [50] S. Pratt, “Pion lasers from high-energy collisions,” *Phys.Lett.* **B301** (1993) 159–164.
- [51] S. Pratt, “Deciphering the CENTAURO puzzle,” *Phys.Rev.* **C50** (1994) 469–479.
- [52] R. Lednicky, V. Lyuboshitz, K. Mikhailov, Y. Sinyukov, A. Stavinsky, *et al.*, “Multiboson effects in multiparticle production,” *Phys.Rev.* **C61** (2000) 034901, arXiv:nucl-th/9911055 [nucl-th].
- [53] Q. Zhang, P. Scotto, and U. W. Heinz, “Multiboson effects and the normalization of the two pion correlation function,” *Phys.Rev.* **C58** (1998) 3757–3760, arXiv:nucl-th/9805046 [nucl-th].
- [54] Y. Sinyukov, R. Lednicky, S. Akkelin, J. Pluta, and B. Erasmus, “Coulomb corrections for interferometry analysis of expanding hadron systems,” *Phys.Lett.* **B432** (1998) 248–257.

A Appendix

Given the experimentally measured two-pion correlation functions, one may build the expectation for higher order correlation functions using the equations of quantum statistics. The measured two-pion correlation functions are first corrected for experimental distortions: momentum resolution and muon contamination. Corrections for long-lived emitters and FSI are then performed to extract the genuine QS correlation according to $C_2 = (1 - f_c^2) + f_c^2 K_2 C_2^{\text{QS}}$ [54]. In the case of no coherent emission, the pair-exchange magnitudes (T_{ij}) can be extracted according to: $C_2^{\text{QS}} = 1 + T_{ij}^2$. The extracted pair-exchange magnitudes are then used to build the expectation for higher order QS correlations [5, 18, 19]. In the absence of coherent emission and multipion phases, the three- and four-pion expected QS correlations are

$$E_3 = 1 + [T_{12}^2 + \text{c.p.}] + 2T_{12}T_{23}T_{31}, \quad (\text{A.1})$$

$$E_4 = 1 + [T_{12}^2 + \text{c.p.}] + [T_{12}^2 T_{34}^2 + \text{c.p.}] + 2[T_{12}T_{23}T_{31} + \text{c.p.}] + 2[T_{12}T_{23}T_{34}T_{41} + \text{c.p.}], \quad (\text{A.2})$$

where c.p. stands for the cyclically permuted terms. The equations which include partial coherence can be found in Ref. [5, 18, 19]. The T_{ij} factors are tabulated from the first pass over the data and used to build higher order correlations by means of a weight applied to the fully mixed-event distribution in the second and final pass.

Each symmetrization sequence is formed with a product of pair-exchange magnitudes. Single-pair, double-pair, triplet, and quadruplet sequences are represented by $T_{ij}T_{ji}$, $T_{ij}^2 T_{kl}^2$, $T_{ij}T_{jk}T_{ki}$, $T_{ij}T_{jk}T_{kl}T_{li}$, respectively. The sum of the appropriate symmetrization sequences yields the expected versions of C_4^{QS} , a_4^{QS} , b_4^{QS} , and c_4^{QS} .

B The ALICE Collaboration

J. Adam⁴⁰, D. Adamová⁸⁴, M.M. Aggarwal⁸⁸, G. Aglieri Rinella³⁶, M. Agnello¹¹⁰, N. Agrawal⁴⁸, Z. Ahammed¹³², S. Ahmad¹⁹, S.U. Ahn⁶⁸, S. Aiola¹³⁶, A. Akindinov⁵⁸, S.N. Alam¹³², D. Aleksandrov⁸⁰, B. Alessandro¹¹⁰, D. Alexandre¹⁰¹, R. Alfaro Molina⁶⁴, A. Alici^{12,104}, A. Alkin³, J.R.M. Almaraz¹¹⁹, J. Alme³⁸, T. Alt⁴³, S. Altinpinar¹⁸, I. Altsybeev¹³¹, C. Alves Garcia Prado¹²⁰, C. Andrei⁷⁸, A. Andronic⁹⁷, V. Anguelov⁹⁴, T. Antičić⁹⁸, F. Antinori¹⁰⁷, P. Antonioli¹⁰⁴, L. Aphecetche¹¹³, H. Appelshäuser⁵³, S. Arcelli²⁸, R. Arnaldi¹¹⁰, O.W. Arnold^{37,93}, I.C. Arsene²², M. Arslandok⁵³, B. Audurier¹¹³, A. Augustinus³⁶, R. Averbeck⁹⁷, M.D. Azmi¹⁹, A. Badalà¹⁰⁶, Y.W. Baek⁶⁷, S. Bagnasco¹¹⁰, R. Bailhache⁵³, R. Bala⁹¹, S. Balasubramanian¹³⁶, A. Baldisseri¹⁵, R.C. Baral⁶¹, A.M. Barabano²⁷, R. Barbera²⁹, F. Barile³³, G.G. Barnaföldi¹³⁵, L.S. Barnby¹⁰¹, V. Barret⁷⁰, P. Bartalini⁷, K. Barth³⁶, J. Bartke¹¹⁷, E. Bartsch⁵³, M. Basile²⁸, N. Bastid⁷⁰, S. Basu¹³², B. Bathen⁵⁴, G. Batigne¹¹³, A. Batista Camejo⁷⁰, B. Batyunya⁶⁶, P.C. Batzing²², I.G. Bearden⁸¹, H. Beck⁵³, C. Bedda¹¹⁰, N.K. Behera⁵⁰, I. Belikov⁵⁵, F. Bellini²⁸, H. Bello Martinez², R. Bellwied¹²², R. Belmont¹³⁴, E. Belmont-Moreno⁶⁴, V. Belyaev⁷⁵, P. Benacek⁸⁴, G. Bencedi¹³⁵, S. Beole²⁷, I. Berceanu⁷⁸, A. Bercuci⁷⁸, Y. Berdnikov⁸⁶, D. Berenyi¹³⁵, R.A. Bertens⁵⁷, D. Berzano³⁶, L. Betev³⁶, A. Bhasin⁹¹, I.R. Bhat⁹¹, A.K. Bhati⁸⁸, B. Bhattacharjee⁴⁵, J. Bhom¹²⁸, L. Bianchi¹²², N. Bianchi⁷², C. Bianchin^{134,57}, J. Bielčík⁴⁰, J. Bielčíková⁸⁴, A. Bilandzic^{81,37,93}, G. Biro¹³⁵, R. Biswas⁴, S. Biswas⁷⁹, S. Bjelogrić⁵⁷, J.T. Blair¹¹⁸, D. Blau⁸⁰, C. Blume⁵³, F. Bock^{74,94}, A. Bogdanov⁷⁵, H. Bøggild⁸¹, L. Boldizsár¹³⁵, M. Bombara⁴¹, J. Book⁵³, H. Borel¹⁵, A. Borissov⁹⁶, M. Borri^{83,124}, F. Bossú⁶⁵, E. Botta²⁷, C. Bourjau⁸¹, P. Braun-Munzinger⁹⁷, M. Bregant¹²⁰, T. Breitner⁵², T.A. Broker⁵³, T.A. Browning⁹⁵, M. Broz⁴⁰, E.J. Brucken⁴⁶, E. Bruna¹¹⁰, G.E. Bruno³³, D. Budnikov⁹⁹, H. Buesching⁵³, S. Bufalino^{36,27}, P. Buncic³⁶, O. Busch^{94,128}, Z. Buthelezi⁶⁵, J.B. Butt¹⁶, J.T. Buxton²⁰, D. Caffarri³⁶, X. Cai⁷, H. Caines¹³⁶, L. Calero Diaz⁷², A. Caliva⁵⁷, E. Calvo Villar¹⁰², P. Camerini²⁶, F. Carena³⁶, W. Carena³⁶, F. Carnesecchi²⁸, J. Castillo Castellanos¹⁵, A.J. Castro¹²⁵, E.A.R. Casula²⁵, C. Ceballos Sanchez⁹, P. Cerello¹¹⁰, J. Cerkala¹¹⁵, B. Chang¹²³, S. Chapeland³⁶, M. Chartier¹²⁴, J.L. Charvet¹⁵, S. Chattopadhyay¹³², S. Chattopadhyay¹⁰⁰, A. Chauvin^{93,37}, V. Chelnokov³, M. Cherney⁸⁷, C. Cheshkov¹³⁰, B. Cheynis¹³⁰, V. Chibante Barroso³⁶, D.D. Chinellato¹²¹, S. Cho⁵⁰, P. Chochula³⁶, K. Choi⁹⁶, M. Chojnacki⁸¹, S. Choudhury¹³², P. Christakoglou⁸², C.H. Christensen⁸¹, P. Christiansen³⁴, T. Chujo¹²⁸, S.U. Chung⁹⁶, C. Cicalo¹⁰⁵, L. Cifarelli^{12,28}, F. Cindolo¹⁰⁴, J. Cleymans⁹⁰, F. Colamaria³³, D. Colella^{59,36}, A. Collu^{74,25}, M. Colocci²⁸, G. Conesa Balbastre⁷¹, Z. Conesa del Valle⁵¹, M.E. Connors^{ii,136}, J.G. Contreras⁴⁰, T.M. Cormier⁸⁵, Y. Corrales Morales¹¹⁰, I. Cortés Maldonado², P. Cortese³², M.R. Cosentino¹²⁰, F. Costa³⁶, P. Crochet⁷⁰, R. Cruz Albino¹¹, E. Cuautele⁶³, L. Cunqueiro^{54,36}, T. Dahms^{93,37}, A. Dainese¹⁰⁷, M.C. Danisch⁹⁴, A. Danu⁶², D. Das¹⁰⁰, I. Das¹⁰⁰, S. Das⁴, A. Dash^{121,79}, S. Dash⁴⁸, S. De¹²⁰, A. De Caro^{12,31}, G. de Cataldo¹⁰³, C. de Conti¹²⁰, J. de Cuveland⁴³, A. De Falco²⁵, D. De Gruttola^{12,31}, N. De Marco¹¹⁰, S. De Pasquale³¹, A. Deisting^{97,94}, A. Deloff⁷⁷, E. Dénes^{135,i}, C. Deplano⁸², P. Dhankher⁴⁸, D. Di Bari³³, A. Di Mauro³⁶, P. Di Nezza⁷², M.A. Diaz Corchero¹⁰, T. Dietel⁹⁰, P. Dillenseger⁵³, R. Divià³⁶, Ø. Djuvsland¹⁸, A. Dobrin^{62,82}, D. Domenicis Gimenez¹²⁰, B. Dönigus⁵³, O. Dordic²², T. Drozhzhova⁵³, A.K. Dubey¹³², A. Dubla⁵⁷, L. Ducroux¹³⁰, P. Dupieux⁷⁰, R.J. Ehlers¹³⁶, D. Elia¹⁰³, E. Endress¹⁰², H. Engel⁵², E. Eppele¹³⁶, B. Erazmus¹¹³, I. Erdemir⁵³, F. Erhardt¹²⁹, B. Espagnon⁵¹, M. Estienne¹¹³, S. Esumi¹²⁸, J. Eum⁹⁶, D. Evans¹⁰¹, S. Evdokimov¹¹¹, G. Eyyubova⁴⁰, L. Fabbietti^{93,37}, D. Fabris¹⁰⁷, J. Faivre⁷¹, A. Fantoni⁷², M. Fasel⁷⁴, L. Feldkamp⁵⁴, A. Feliciello¹¹⁰, G. Feofilov¹³¹, J. Ferencei⁸⁴, A. Fernández Téllez², E.G. Ferreira¹⁷, A. Ferretti²⁷, A. Festanti³⁰, V.J.G. Feuillard^{15,70}, J. Figiel¹¹⁷, M.A.S. Figueredo^{124,120}, S. Filchagin⁹⁹, D. Finogeev⁵⁶, F.M. Fionda²⁵, E.M. Fiore³³, M.G. Fleck⁹⁴, M. Floris³⁶, S. Foertsch⁶⁵, P. Foka⁹⁷, S. Fokin⁸⁰, E. Fragiaco¹⁰⁹, A. Francescon^{36,30}, U. Frankenfeld⁹⁷, G.G. Fronze²⁷, U. Fuchs³⁶, C. Furget⁷¹, A. Furs⁵⁶, M. Fusco Girard³¹, J.J. Gaardhøje⁸¹, M. Gagliardi²⁷, A.M. Gago¹⁰², M. Gallio²⁷, D.R. Gangadharan⁷⁴, P. Ganoti⁸⁹, C. Gao⁷, C. Garabatos⁹⁷, E. Garcia-Solis¹³,

C. Gargiulo³⁶, P. Gasik^{93,37}, E.F. Gauger¹¹⁸, M. Germain¹¹³, A. Gheata³⁶, M. Gheata^{36,62}, P. Ghosh¹³², S.K. Ghosh⁴, P. Gianotti⁷², P. Giubellino^{110,36}, P. Giubilato³⁰, E. Gladysz-Dziadus¹¹⁷, P. Glässel⁹⁴, D.M. Gómez Coral⁶⁴, A. Gomez Ramirez⁵², V. Gonzalez¹⁰, P. González-Zamora¹⁰, S. Gorbunov⁴³, L. Görlich¹¹⁷, S. Gotovac¹¹⁶, V. Grabski⁶⁴, O.A. Grachov¹³⁶, L.K. Graczykowski¹³³, K.L. Graham¹⁰¹, A. Grelli⁵⁷, A. Grigoras³⁶, C. Grigoras³⁶, V. Grigoriev⁷⁵, A. Grigoryan¹, S. Grigoryan⁶⁶, B. Grinyov³, N. Grion¹⁰⁹, J.M. Gronefeld⁹⁷, J.F. Grosse-Oetringhaus³⁶, J.-Y. Grossiord¹³⁰, R. Grosso⁹⁷, F. Guber⁵⁶, R. Guernane⁷¹, B. Guerzoni²⁸, K. Gulbrandsen⁸¹, T. Gunji¹²⁷, A. Gupta⁹¹, R. Gupta⁹¹, R. Haake⁵⁴, Ø. Haaland¹⁸, C. Hadjidakis⁵¹, M. Haiduc⁶², H. Hamagaki¹²⁷, G. Hamar¹³⁵, J.C. Hamon⁵⁵, J.W. Harris¹³⁶, A. Harton¹³, D. Hatzifotiadou¹⁰⁴, S. Hayashi¹²⁷, S.T. Heckel⁵³, H. Helstrup³⁸, A. Herghelegiu⁷⁸, G. Herrera Corral¹¹, B.A. Hess³⁵, K.F. Hetland³⁸, H. Hillemanns³⁶, B. Hippolyte⁵⁵, D. Horak⁴⁰, R. Hosokawa¹²⁸, P. Hristov³⁶, M. Huang¹⁸, T.J. Humanic²⁰, N. Hussain⁴⁵, T. Hussain¹⁹, D. Hutter⁴³, D.S. Hwang²¹, R. Ilkaev⁹⁹, M. Inaba¹²⁸, E. Incani²⁵, M. Ippolitov^{75,80}, M. Irfan¹⁹, M. Ivanov⁹⁷, V. Ivanov⁸⁶, V. Izucheev¹¹¹, N. Jacazio²⁸, P.M. Jacobs⁷⁴, M.B. Jadhav⁴⁸, S. Jadlovská¹¹⁵, J. Jadlovsky^{115,59}, C. Jahnke¹²⁰, M.J. Jakubowska¹³³, H.J. Jang⁶⁸, M.A. Janik¹³³, P.H.S.Y. Jayarathna¹²², C. Jena³⁰, S. Jena¹²², R.T. Jimenez Bustamante⁹⁷, P.G. Jones¹⁰¹, A. Jusko¹⁰¹, P. Kalinak⁵⁹, A. Kalweit³⁶, J. Kamin⁵³, J.H. Kang¹³⁷, V. Kaplin⁷⁵, S. Kar¹³², A. Karasu Uysal⁶⁹, O. Karavichev⁵⁶, T. Karavicheva⁵⁶, L. Karayan^{97,94}, E. Karpechev⁵⁶, U. Kebschull⁵², R. Keidel¹³⁸, D.L.D. Keijdener⁵⁷, M. Keil³⁶, M. Mohisin Khan^{iii,19}, P. Khan¹⁰⁰, S.A. Khan¹³², A. Khanzadeev⁸⁶, Y. Kharlov¹¹¹, B. Kileng³⁸, D.W. Kim⁴⁴, D.J. Kim¹²³, D. Kim¹³⁷, H. Kim¹³⁷, J.S. Kim⁴⁴, M. Kim¹³⁷, S. Kim²¹, T. Kim¹³⁷, S. Kirsch⁴³, I. Kisel⁴³, S. Kiselev⁵⁸, A. Kisiel¹³³, G. Kiss¹³⁵, J.L. Klay⁶, C. Klein⁵³, J. Klein³⁶, C. Klein-Bösing⁵⁴, S. Klewin⁹⁴, A. Kluge³⁶, M.L. Knichel⁹⁴, A.G. Knospe¹¹⁸, C. Kobdaj¹¹⁴, M. Kofarago³⁶, T. Kollegger⁹⁷, A. Kolojvari¹³¹, V. Kondratiev¹³¹, N. Kondratyeva⁷⁵, E. Kondratyuk¹¹¹, A. Konevskikh⁵⁶, M. Kopicik¹¹⁵, P. Kostarakis⁸⁹, M. Kour⁹¹, C. Kouzinopoulos³⁶, O. Kovalenko⁷⁷, V. Kovalenko¹³¹, M. Kowalski¹¹⁷, G. Koyithatta Meethalevedu⁴⁸, I. Králik⁵⁹, A. Kravčáková⁴¹, M. Kretz⁴³, M. Krivda^{59,101}, F. Krizek⁸⁴, E. Kryshen^{86,36}, M. Krzewicki⁴³, A.M. Kubera²⁰, V. Kučera⁸⁴, C. Kuhn⁵⁵, P.G. Kuijer⁸², A. Kumar⁹¹, J. Kumar⁴⁸, L. Kumar⁸⁸, S. Kumar⁴⁸, P. Kurashvili⁷⁷, A. Kurepin⁵⁶, A.B. Kurepin⁵⁶, A. Kuryakin⁹⁹, M.J. Kweon⁵⁰, Y. Kwon¹³⁷, S.L. La Pointe¹¹⁰, P. La Rocca²⁹, P. Ladron de Guevara¹¹, C. Lagana Fernandes¹²⁰, I. Lakomov³⁶, R. Langoy⁴², C. Lara⁵², A. Lardeux¹⁵, A. Lattuca²⁷, E. Laudi³⁶, R. Lea²⁶, L. Leardini⁹⁴, G.R. Lee¹⁰¹, S. Lee¹³⁷, F. Lehas⁸², R.C. Lemmon⁸³, V. Lenti¹⁰³, E. Leogrande⁵⁷, I. León Monzón¹¹⁹, H. León Vargas⁶⁴, M. Leoncino²⁷, P. Lévai¹³⁵, S. Li^{7,70}, X. Li¹⁴, J. Lien⁴², R. Lietava¹⁰¹, S. Lindal²², V. Lindenstruth⁴³, C. Lippmann⁹⁷, M.A. Lisa²⁰, H.M. Ljunggren³⁴, D.F. Lodato⁵⁷, P.I. Loenne¹⁸, V. Loginov⁷⁵, C. Loizides⁷⁴, X. Lopez⁷⁰, E. López Torres⁹, A. Lowe¹³⁵, P. Luettig⁵³, M. Lunardon³⁰, G. Luparello²⁶, T.H. Lutz¹³⁶, A. Maevskaya⁵⁶, M. Mager³⁶, S. Mahajan⁹¹, S.M. Mahmood²², A. Maire⁵⁵, R.D. Majka¹³⁶, M. Malaev⁸⁶, I. Maldonado Cervantes⁶³, L. Malinina^{iv,66}, D. Mal'Kevich⁵⁸, P. Malzacher⁹⁷, A. Mamonov⁹⁹, V. Manko⁸⁰, F. Manso⁷⁰, V. Manzari^{36,103}, M. Marchisone^{27,65,126}, J. Mareš⁶⁰, G.V. Margagliotti²⁶, A. Margotti¹⁰⁴, J. Margutti⁵⁷, A. Marín⁹⁷, C. Markert¹¹⁸, M. Marquard⁵³, N.A. Martin⁹⁷, J. Martin Blanco¹¹³, P. Martinengo³⁶, M.I. Martínez², G. Martínez García¹¹³, M. Martinez Pedreira³⁶, A. Mas¹²⁰, S. Masciocchi⁹⁷, M. Masera²⁷, A. Masoni¹⁰⁵, L. Massacrier¹¹³, A. Mastroserio³³, A. Matyja¹¹⁷, C. Mayer^{117,36}, J. Mazer¹²⁵, M.A. Mazzone¹⁰⁸, D. McDonald¹²², F. Meddi²⁴, Y. Melikyan⁷⁵, A. Menchaca-Rocha⁶⁴, E. Meninno³¹, J. Mercado Pérez⁹⁴, M. Meres³⁹, Y. Miake¹²⁸, M.M. Mieskolainen⁴⁶, K. Mikhaylov^{66,58}, L. Milano^{74,36}, J. Milosevic²², L.M. Minervini^{103,23}, A. Mischke⁵⁷, A.N. Mishra⁴⁹, D. Miśkowiec⁹⁷, J. Mitra¹³², C.M. Mitu⁶², N. Mohammadi⁵⁷, B. Mohanty^{79,132}, L. Molnar^{55,113}, L. Montaño Zetina¹¹, E. Montes¹⁰, D.A. Moreira De Godoy^{113,54}, L.A.P. Moreno², S. Moretto³⁰, A. Morreale¹¹³, A. Morsch³⁶, V. Muccifora⁷², E. Mudnic¹¹⁶, D. Mühlheim⁵⁴, S. Muhuri¹³², M. Mukherjee¹³², J.D. Mulligan¹³⁶, M.G. Munhoz¹²⁰, R.H. Munzer^{37,93}, H. Murakami¹²⁷, S. Murray⁶⁵, L. Musa³⁶, J. Musinsky⁵⁹, B. Naik⁴⁸, R. Nair⁷⁷, B.K. Nandi⁴⁸, R. Nania¹⁰⁴, E. Nappi¹⁰³, M.U. Naru¹⁶, H. Natal da Luz¹²⁰, C. Nattrass¹²⁵,

S.R. Navarro², K. Nayak⁷⁹, R. Nayak⁴⁸, T.K. Nayak¹³², S. Nazarenko⁹⁹, A. Nedosekin⁵⁸, L. Nellen⁶³, F. Ng¹²², M. Nicassio⁹⁷, M. Niculescu⁶², J. Niedziela³⁶, B.S. Nielsen⁸¹, S. Nikolaev⁸⁰, S. Nikulin⁸⁰, V. Nikulin⁸⁶, F. Noferini^{104,12}, P. Nomokonov⁶⁶, G. Nooren⁵⁷, J.C.C. Noris², J. Norman¹²⁴, A. Nyanin⁸⁰, J. Nystrand¹⁸, H. Oeschler⁹⁴, S. Oh¹³⁶, S.K. Oh⁶⁷, A. Ohlson³⁶, A. Okatan⁶⁹, T. Okubo⁴⁷, L. Olah¹³⁵, J. Oleniacz¹³³, A.C. Oliveira Da Silva¹²⁰, M.H. Oliver¹³⁶, J. Onderwaater⁹⁷, C. Oppedisano¹¹⁰, R. Orava⁴⁶, A. Ortiz Velasquez⁶³, A. Oskarsson³⁴, J. Otwinowski¹¹⁷, K. Oyama^{94,76}, M. Ozdemir⁵³, Y. Pachmayer⁹⁴, P. Pagano³¹, G. Paic⁶³, S.K. Pal¹³², J. Pan¹³⁴, A.K. Pandey⁴⁸, V. Papikyan¹, G.S. Pappalardo¹⁰⁶, P. Pareek⁴⁹, W.J. Park⁹⁷, S. Parmar⁸⁸, A. Passfeld⁵⁴, V. Paticchio¹⁰³, R.N. Patra¹³², B. Paul¹⁰⁰, H. Pei⁷, T. Peitzmann⁵⁷, H. Pereira Da Costa¹⁵, D. Peresunko^{80,75}, C.E. Pérez Lara⁸², E. Perez Lezama⁵³, V. Peskov⁵³, Y. Pestov⁵, V. Petráček⁴⁰, V. Petrov¹¹¹, M. Petrovici⁷⁸, C. Petta²⁹, S. Piano¹⁰⁹, M. Pikna³⁹, P. Pillot¹¹³, L.O.D.L. Pimentel⁸¹, O. Pinazza^{36,104}, L. Pinsky¹²², D.B. Piyarathna¹²², M. Płoskoń⁷⁴, M. Planinic¹²⁹, J. Pluta¹³³, S. Pochybova¹³⁵, P.L.M. Podesta-Lerma¹¹⁹, M.G. Poghosyan^{85,87}, B. Polichtchouk¹¹¹, N. Poljak¹²⁹, W. Poonsawat¹¹⁴, A. Pop⁷⁸, S. Porteboeuf-Houssais⁷⁰, J. Porter⁷⁴, J. Pospisil⁸⁴, S.K. Prasad⁴, R. Preghenella^{104,36}, F. Prino¹¹⁰, C.A. Pruneau¹³⁴, I. Pshenichnov⁵⁶, M. Puccio²⁷, G. Puudu²⁵, P. Pujahari¹³⁴, V. Punin⁹⁹, J. Putschke¹³⁴, H. Qvigstad²², A. Rachevski¹⁰⁹, S. Raha⁴, S. Rajput⁹¹, J. Rak¹²³, A. Rakotozafindrabe¹⁵, L. Ramello³², F. Rami⁵⁵, R. Raniwala⁹², S. Raniwala⁹², S.S. Räsänen⁴⁶, B.T. Rascanu⁵³, D. Rathee⁸⁸, K.F. Read^{85,125}, K. Redlich⁷⁷, R.J. Reed¹³⁴, A. Rehman¹⁸, P. Reichelt⁵³, F. Reidt^{94,36}, X. Ren⁷, R. Renfordt⁵³, A.R. Reolon⁷², A. Reshetin⁵⁶, J.-P. Revol¹², K. Reygers⁹⁴, V. Riabov⁸⁶, R.A. Ricci⁷³, T. Richert³⁴, M. Richter²², P. Riedler³⁶, W. Riegler³⁶, F. Riggi²⁹, C. Ristea⁶², E. Rocco⁵⁷, M. Rodríguez Cahuantzi^{11,2}, A. Rodriguez Manso⁸², K. Røed²², E. Rogochaya⁶⁶, D. Rohr⁴³, D. Röhrich¹⁸, R. Romita¹²⁴, F. Ronchetti^{72,36}, L. Ronflette¹¹³, P. Rosnet⁷⁰, A. Rossi^{36,30}, F. Roukoutakis⁸⁹, A. Roy⁴⁹, C. Roy⁵⁵, P. Roy¹⁰⁰, A.J. Rubio Montero¹⁰, R. Rui²⁶, R. Russo²⁷, E. Ryabinkin⁸⁰, Y. Ryabov⁸⁶, A. Rybicki¹¹⁷, S. Sadovsky¹¹¹, K. Šafařík³⁶, B. Sahlmuller⁵³, P. Sahoo⁴⁹, R. Sahoo⁴⁹, S. Sahoo⁶¹, P.K. Sahu⁶¹, J. Saini¹³², S. Sakai⁷², M.A. Saleh¹³⁴, J. Salzwedel²⁰, S. Sambyal⁹¹, V. Samsonov⁸⁶, L. Šándor⁵⁹, A. Sandoval⁶⁴, M. Sano¹²⁸, D. Sarkar¹³², P. Sarma⁴⁵, E. Scapparone¹⁰⁴, F. Scarlassara³⁰, C. Schiaua⁷⁸, R. Schicker⁹⁴, C. Schmidt⁹⁷, H.R. Schmidt³⁵, S. Schuchmann⁵³, J. Schukraft³⁶, M. Schulc⁴⁰, T. Schuster¹³⁶, Y. Schutz^{36,113}, K. Schwarz⁹⁷, K. Schweda⁹⁷, G. Scioli²⁸, E. Scomparin¹¹⁰, R. Scott¹²⁵, M. Šefčík⁴¹, J.E. Seger⁸⁷, Y. Sekiguchi¹²⁷, D. Sekihata⁴⁷, I. Selyuzhenkov⁹⁷, K. Senosi⁶⁵, S. Senyukov^{3,36}, E. Serradilla^{10,64}, A. Sevcenco⁶², A. Shabanov⁵⁶, A. Shabetai¹¹³, O. Shadura³, R. Shahoyan³⁶, M.I. Shahzad¹⁶, A. Shangaraev¹¹¹, A. Sharma⁹¹, M. Sharma⁹¹, M. Sharma⁹¹, N. Sharma¹²⁵, K. Shigaki⁴⁷, K. Shtejer^{9,27}, Y. Sibiraki⁸⁰, S. Siddhanta¹⁰⁵, K.M. Sielewicz³⁶, T. Siemiarczuk⁷⁷, D. Silvermyr³⁴, C. Silvestre⁷¹, G. Simatovic¹²⁹, G. Simonetti³⁶, R. Singaraju¹³², R. Singh⁷⁹, S. Singha^{132,79}, V. Singhal¹³², B.C. Sinha¹³², T. Sinha¹⁰⁰, B. Sitar³⁹, M. Sitta³², T.B. Skaali²², M. Slupecki¹²³, N. Smirnov¹³⁶, R.J.M. Snellings⁵⁷, T.W. Snellman¹²³, C. Sogaard³⁴, J. Song⁹⁶, M. Song¹³⁷, Z. Song⁷, F. Soramel³⁰, S. Sorensen¹²⁵, R.D.de Souza¹²¹, F. Sozzi⁹⁷, M. Spacek⁴⁰, E. Spiriti⁷², I. Sputowska¹¹⁷, M. Spyropoulou-Stassinaki⁸⁹, J. Stachel⁹⁴, I. Stan⁶², P. Stankus⁸⁵, G. Stefanek⁷⁷, E. Stenlund³⁴, G. Steyn⁶⁵, J.H. Stiller⁹⁴, D. Stocco¹¹³, P. Strmen³⁹, A.A.P. Suaide¹²⁰, T. Sugitate⁴⁷, C. Suire⁵¹, M. Suleymanov¹⁶, M. Suljic^{26,i}, R. Sultanov⁵⁸, M. Šumbera⁸⁴, A. Szabo³⁹, A. Szanto de Toledo^{120,i}, I. Szarka³⁹, A. Szczepankiewicz³⁶, M. Szymanski¹³³, U. Tabassam¹⁶, J. Takahashi¹²¹, G.J. Tambave¹⁸, N. Tanaka¹²⁸, M.A. Tangaro³³, M. Tarhini⁵¹, M. Tariq¹⁹, M.G. Tarzila⁷⁸, A. Tauro³⁶, G. Tejeda Muñoz², A. Telesca³⁶, K. Terasaki¹²⁷, C. Terrevoli³⁰, B. Teyssier¹³⁰, J. Thäder⁷⁴, D. Thomas¹¹⁸, R. Tieulent¹³⁰, A.R. Timmins¹²², A. Toia⁵³, S. Trogolo²⁷, G. Trombetta³³, V. Trubnikov³, W.H. Trzaska¹²³, T. Tsuji¹²⁷, A. Tumkin⁹⁹, R. Turrisi¹⁰⁷, T.S. Tveter²², K. Ullaland¹⁸, A. Uras¹³⁰, G.L. Usai²⁵, A. Utrobicic¹²⁹, M. Vajzer⁸⁴, M. Vala⁵⁹, L. Valencia Palomo⁷⁰, S. Vallero²⁷, J. Van Der Maarel⁵⁷, J.W. Van Hoorne³⁶, M. van Leeuwen⁵⁷, T. Vanat⁸⁴, P. Vande Vyvre³⁶, D. Varga¹³⁵, A. Vargas², M. Vargyas¹²³, R. Varma⁴⁸, M. Vasileiou⁸⁹, A. Vasiliev⁸⁰, A. Vauthier⁷¹, V. Vechemin¹³¹, A.M. Veen⁵⁷, M. Veldhoen⁵⁷, A. Velure¹⁸,

M. Venaruzzo⁷³, E. Vercellin²⁷, S. Vergara Limón², R. Vernet⁸, M. Verweij¹³⁴, L. Vickovic¹¹⁶, G. Viesti^{30, i}, J. Viinikainen¹²³, Z. Vilakazi¹²⁶, O. Villalobos Baillie¹⁰¹, A. Villatoro Tello², A. Vinogradov⁸⁰, L. Vinogradov¹³¹, Y. Vinogradov^{99, i}, T. Virgili³¹, V. Vislavicius³⁴, Y.P. Viyogi¹³², A. Vodopyanov⁶⁶, M.A. Völkl⁹⁴, K. Voloshin⁵⁸, S.A. Voloshin¹³⁴, G. Volpe³³, B. von Haller³⁶, I. Vorobyev^{37, 93}, D. Vranic^{97, 36}, J. Vrláková⁴¹, B. Vulpescu⁷⁰, B. Wagner¹⁸, J. Wagner⁹⁷, H. Wang⁵⁷, M. Wang^{7, 113}, D. Watanabe¹²⁸, Y. Watanabe¹²⁷, M. Weber^{36, 112}, S.G. Weber⁹⁷, D.F. Weiser⁹⁴, J.P. Wessels⁵⁴, U. Westerhoff⁵⁴, A.M. Whitehead⁹⁰, J. Wiechula³⁵, J. Wikne²², G. Wilk⁷⁷, J. Wilkinson⁹⁴, M.C.S. Williams¹⁰⁴, B. Windelband⁹⁴, M. Winn⁹⁴, H. Yang⁵⁷, P. Yang⁷, S. Yano⁴⁷, Z. Yasin¹⁶, Z. Yin⁷, H. Yokoyama¹²⁸, I.-K. Yoo⁹⁶, J.H. Yoon⁵⁰, V. Yurchenko³, I. Yushmanov⁸⁰, A. Zaborowska¹³³, V. Zaccolo⁸¹, A. Zaman¹⁶, C. Zampolli^{36, 104}, H.J.C. Zanoli¹²⁰, S. Zaporozhets⁶⁶, N. Zardoshti¹⁰¹, A. Zarochentsev¹³¹, P. Závada⁶⁰, N. Zaviyalov⁹⁹, H. Zbroszczyk¹³³, I.S. Zgura⁶², M. Zhalov⁸⁶, H. Zhang¹⁸, X. Zhang⁷⁴, Y. Zhang⁷, C. Zhang⁵⁷, Z. Zhang⁷, C. Zhao²², N. Zhigareva⁵⁸, D. Zhou⁷, Y. Zhou⁸¹, Z. Zhou¹⁸, H. Zhu¹⁸, J. Zhu^{113, 7}, A. Zichichi^{28, 12}, A. Zimmermann⁹⁴, M.B. Zimmermann^{54, 36}, G. Zinovjev³, M. Zyzak⁴³

Affiliation notes

ⁱ Deceased

ⁱⁱ Also at: Georgia State University, Atlanta, Georgia, United States

ⁱⁱⁱ Also at: Also at Department of Applied Physics, Aligarh Muslim University, Aligarh, India

^{iv} Also at: M.V. Lomonosov Moscow State University, D.V. Skobeltsyn Institute of Nuclear Physics, Moscow, Russia

Collaboration Institutes

¹ A.I. Alikhanyan National Science Laboratory (Yerevan Physics Institute) Foundation, Yerevan, Armenia

² Benemérita Universidad Autónoma de Puebla, Puebla, Mexico

³ Bogolyubov Institute for Theoretical Physics, Kiev, Ukraine

⁴ Bose Institute, Department of Physics and Centre for Astroparticle Physics and Space Science (CAPSS), Kolkata, India

⁵ Budker Institute for Nuclear Physics, Novosibirsk, Russia

⁶ California Polytechnic State University, San Luis Obispo, California, United States

⁷ Central China Normal University, Wuhan, China

⁸ Centre de Calcul de l'IN2P3, Villeurbanne, France

⁹ Centro de Aplicaciones Tecnológicas y Desarrollo Nuclear (CEADEN), Havana, Cuba

¹⁰ Centro de Investigaciones Energéticas Medioambientales y Tecnológicas (CIEMAT), Madrid, Spain

¹¹ Centro de Investigación y de Estudios Avanzados (CINVESTAV), Mexico City and Mérida, Mexico

¹² Centro Fermi - Museo Storico della Fisica e Centro Studi e Ricerche "Enrico Fermi", Rome, Italy

¹³ Chicago State University, Chicago, Illinois, USA

¹⁴ China Institute of Atomic Energy, Beijing, China

¹⁵ Commissariat à l'Énergie Atomique, IRFU, Saclay, France

¹⁶ COMSATS Institute of Information Technology (CIIT), Islamabad, Pakistan

¹⁷ Departamento de Física de Partículas and IGFAE, Universidad de Santiago de Compostela, Santiago de Compostela, Spain

¹⁸ Department of Physics and Technology, University of Bergen, Bergen, Norway

¹⁹ Department of Physics, Aligarh Muslim University, Aligarh, India

²⁰ Department of Physics, Ohio State University, Columbus, Ohio, United States

- 21 Department of Physics, Sejong University, Seoul, South Korea
- 22 Department of Physics, University of Oslo, Oslo, Norway
- 23 Dipartimento di Elettrotecnica ed Elettronica del Politecnico, Bari, Italy
- 24 Dipartimento di Fisica dell'Università 'La Sapienza' and Sezione INFN Rome, Italy
- 25 Dipartimento di Fisica dell'Università and Sezione INFN, Cagliari, Italy
- 26 Dipartimento di Fisica dell'Università and Sezione INFN, Trieste, Italy
- 27 Dipartimento di Fisica dell'Università and Sezione INFN, Turin, Italy
- 28 Dipartimento di Fisica e Astronomia dell'Università and Sezione INFN, Bologna, Italy
- 29 Dipartimento di Fisica e Astronomia dell'Università and Sezione INFN, Catania, Italy
- 30 Dipartimento di Fisica e Astronomia dell'Università and Sezione INFN, Padova, Italy
- 31 Dipartimento di Fisica 'E.R. Caianiello' dell'Università and Gruppo Collegato INFN, Salerno, Italy
- 32 Dipartimento di Scienze e Innovazione Tecnologica dell'Università del Piemonte Orientale and Gruppo Collegato INFN, Alessandria, Italy
- 33 Dipartimento Interateneo di Fisica 'M. Merlin' and Sezione INFN, Bari, Italy
- 34 Division of Experimental High Energy Physics, University of Lund, Lund, Sweden
- 35 Eberhard Karls Universität Tübingen, Tübingen, Germany
- 36 European Organization for Nuclear Research (CERN), Geneva, Switzerland
- 37 Excellence Cluster Universe, Technische Universität München, Munich, Germany
- 38 Faculty of Engineering, Bergen University College, Bergen, Norway
- 39 Faculty of Mathematics, Physics and Informatics, Comenius University, Bratislava, Slovakia
- 40 Faculty of Nuclear Sciences and Physical Engineering, Czech Technical University in Prague, Prague, Czech Republic
- 41 Faculty of Science, P.J. Šafárik University, Košice, Slovakia
- 42 Faculty of Technology, Buskerud and Vestfold University College, Vestfold, Norway
- 43 Frankfurt Institute for Advanced Studies, Johann Wolfgang Goethe-Universität Frankfurt, Frankfurt, Germany
- 44 Gangneung-Wonju National University, Gangneung, South Korea
- 45 Gauhati University, Department of Physics, Guwahati, India
- 46 Helsinki Institute of Physics (HIP), Helsinki, Finland
- 47 Hiroshima University, Hiroshima, Japan
- 48 Indian Institute of Technology Bombay (IIT), Mumbai, India
- 49 Indian Institute of Technology Indore, Indore (IITI), India
- 50 Inha University, Incheon, South Korea
- 51 Institut de Physique Nucléaire d'Orsay (IPNO), Université Paris-Sud, CNRS-IN2P3, Orsay, France
- 52 Institut für Informatik, Johann Wolfgang Goethe-Universität Frankfurt, Frankfurt, Germany
- 53 Institut für Kernphysik, Johann Wolfgang Goethe-Universität Frankfurt, Frankfurt, Germany
- 54 Institut für Kernphysik, Westfälische Wilhelms-Universität Münster, Münster, Germany
- 55 Institut Pluridisciplinaire Hubert Curien (IPHC), Université de Strasbourg, CNRS-IN2P3, Strasbourg, France
- 56 Institute for Nuclear Research, Academy of Sciences, Moscow, Russia
- 57 Institute for Subatomic Physics of Utrecht University, Utrecht, Netherlands
- 58 Institute for Theoretical and Experimental Physics, Moscow, Russia
- 59 Institute of Experimental Physics, Slovak Academy of Sciences, Košice, Slovakia
- 60 Institute of Physics, Academy of Sciences of the Czech Republic, Prague, Czech Republic
- 61 Institute of Physics, Bhubaneswar, India
- 62 Institute of Space Science (ISS), Bucharest, Romania
- 63 Instituto de Ciencias Nucleares, Universidad Nacional Autónoma de México, Mexico City, Mexico

- 64 Instituto de Física, Universidad Nacional Autónoma de México, Mexico City, Mexico
- 65 iThemba LABS, National Research Foundation, Somerset West, South Africa
- 66 Joint Institute for Nuclear Research (JINR), Dubna, Russia
- 67 Konkuk University, Seoul, South Korea
- 68 Korea Institute of Science and Technology Information, Daejeon, South Korea
- 69 KTO Karatay University, Konya, Turkey
- 70 Laboratoire de Physique Corpusculaire (LPC), Clermont Université, Université Blaise Pascal, CNRS-IN2P3, Clermont-Ferrand, France
- 71 Laboratoire de Physique Subatomique et de Cosmologie, Université Grenoble-Alpes, CNRS-IN2P3, Grenoble, France
- 72 Laboratori Nazionali di Frascati, INFN, Frascati, Italy
- 73 Laboratori Nazionali di Legnaro, INFN, Legnaro, Italy
- 74 Lawrence Berkeley National Laboratory, Berkeley, California, United States
- 75 Moscow Engineering Physics Institute, Moscow, Russia
- 76 Nagasaki Institute of Applied Science, Nagasaki, Japan
- 77 National Centre for Nuclear Studies, Warsaw, Poland
- 78 National Institute for Physics and Nuclear Engineering, Bucharest, Romania
- 79 National Institute of Science Education and Research, Bhubaneswar, India
- 80 National Research Centre Kurchatov Institute, Moscow, Russia
- 81 Niels Bohr Institute, University of Copenhagen, Copenhagen, Denmark
- 82 Nikhef, Nationaal instituut voor subatomaire fysica, Amsterdam, Netherlands
- 83 Nuclear Physics Group, STFC Daresbury Laboratory, Daresbury, United Kingdom
- 84 Nuclear Physics Institute, Academy of Sciences of the Czech Republic, Řež u Prahy, Czech Republic
- 85 Oak Ridge National Laboratory, Oak Ridge, Tennessee, United States
- 86 Petersburg Nuclear Physics Institute, Gatchina, Russia
- 87 Physics Department, Creighton University, Omaha, Nebraska, United States
- 88 Physics Department, Panjab University, Chandigarh, India
- 89 Physics Department, University of Athens, Athens, Greece
- 90 Physics Department, University of Cape Town, Cape Town, South Africa
- 91 Physics Department, University of Jammu, Jammu, India
- 92 Physics Department, University of Rajasthan, Jaipur, India
- 93 Physik Department, Technische Universität München, Munich, Germany
- 94 Physikalisches Institut, Ruprecht-Karls-Universität Heidelberg, Heidelberg, Germany
- 95 Purdue University, West Lafayette, Indiana, United States
- 96 Pusan National University, Pusan, South Korea
- 97 Research Division and ExtreMe Matter Institute EMMI, GSI Helmholtzzentrum für Schwerionenforschung, Darmstadt, Germany
- 98 Rudjer Bošković Institute, Zagreb, Croatia
- 99 Russian Federal Nuclear Center (VNIIEF), Sarov, Russia
- 100 Saha Institute of Nuclear Physics, Kolkata, India
- 101 School of Physics and Astronomy, University of Birmingham, Birmingham, United Kingdom
- 102 Sección Física, Departamento de Ciencias, Pontificia Universidad Católica del Perú, Lima, Peru
- 103 Sezione INFN, Bari, Italy
- 104 Sezione INFN, Bologna, Italy
- 105 Sezione INFN, Cagliari, Italy
- 106 Sezione INFN, Catania, Italy
- 107 Sezione INFN, Padova, Italy
- 108 Sezione INFN, Rome, Italy
- 109 Sezione INFN, Trieste, Italy

- 110 Sezione INFN, Turin, Italy
- 111 SSC IHEP of NRC Kurchatov institute, Protvino, Russia
- 112 Stefan Meyer Institut für Subatomare Physik (SMI), Vienna, Austria
- 113 SUBATECH, Ecole des Mines de Nantes, Université de Nantes, CNRS-IN2P3, Nantes, France
- 114 Suranaree University of Technology, Nakhon Ratchasima, Thailand
- 115 Technical University of Košice, Košice, Slovakia
- 116 Technical University of Split FESB, Split, Croatia
- 117 The Henryk Niewodniczanski Institute of Nuclear Physics, Polish Academy of Sciences, Cracow, Poland
- 118 The University of Texas at Austin, Physics Department, Austin, Texas, USA
- 119 Universidad Autónoma de Sinaloa, Culiacán, Mexico
- 120 Universidade de São Paulo (USP), São Paulo, Brazil
- 121 Universidade Estadual de Campinas (UNICAMP), Campinas, Brazil
- 122 University of Houston, Houston, Texas, United States
- 123 University of Jyväskylä, Jyväskylä, Finland
- 124 University of Liverpool, Liverpool, United Kingdom
- 125 University of Tennessee, Knoxville, Tennessee, United States
- 126 University of the Witwatersrand, Johannesburg, South Africa
- 127 University of Tokyo, Tokyo, Japan
- 128 University of Tsukuba, Tsukuba, Japan
- 129 University of Zagreb, Zagreb, Croatia
- 130 Université de Lyon, Université Lyon 1, CNRS/IN2P3, IPN-Lyon, Villeurbanne, France
- 131 V. Fock Institute for Physics, St. Petersburg State University, St. Petersburg, Russia
- 132 Variable Energy Cyclotron Centre, Kolkata, India
- 133 Warsaw University of Technology, Warsaw, Poland
- 134 Wayne State University, Detroit, Michigan, United States
- 135 Wigner Research Centre for Physics, Hungarian Academy of Sciences, Budapest, Hungary
- 136 Yale University, New Haven, Connecticut, United States
- 137 Yonsei University, Seoul, South Korea
- 138 Zentrum für Technologietransfer und Telekommunikation (ZTT), Fachhochschule Worms, Worms, Germany